Article

Cell Reports

Mutual Zonated Interactions of Wnt and Hh Signaling Are Orchestrating the Metabolism of the Adult Liver in Mice and Human

Graphical Abstract

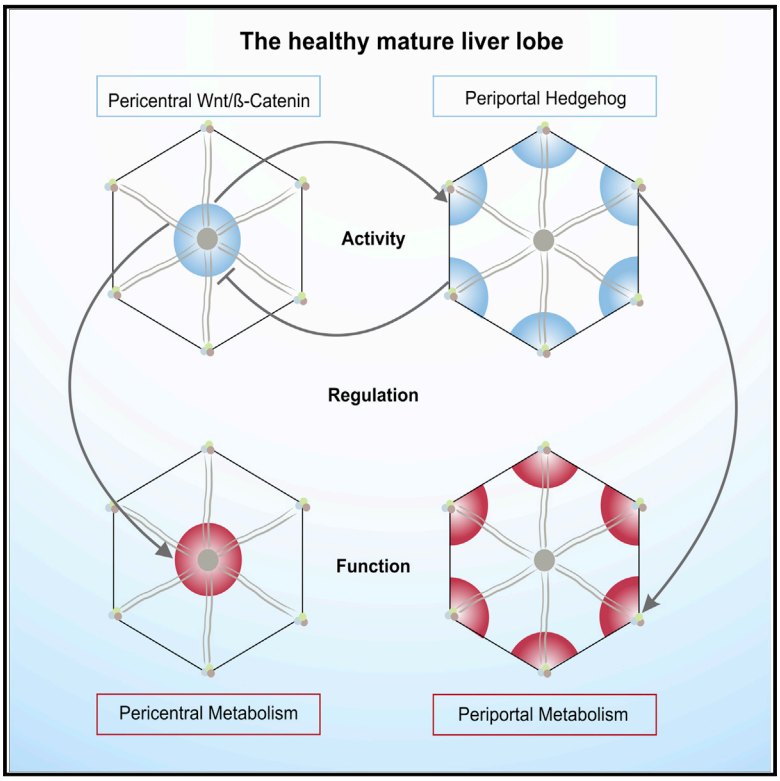

Highlights

- The Hh and Wnt pathways in healthy liver act largely complementary to each other
- The Wnt/Hh module inversely controls spatiotemporal metabolic pathways in the liver
- Inhibition of the Hh pathway leads to periportalization of the liver lobe
- Liver-derived IHH seems to signal to other peripheral organs

Authors

Erik Kolbe, Susanne Aleithe, Christiane Rennert, ..., Jochen Hampe, Rolf Gebhardt, Madlen Matz-Soja

Correspondence

madlen.matz@medizin.uni-leipzig.de

In Brief

Wnt/β-catenin and Hh signaling contribute to embryogenesis as well as to the maintenance of organ homeostasis through intensive crosstalk. Here, Kolbe et al. describe that both pathways act largely complementary to each other in the healthy liver and that this crosstalk is responsible for the maintenance of metabolic zonation.

Kolbe et al., 2019, Cell Reports *29*, 4553–4567
December 24, 2019
https://doi.org/10.1016/j.celrep.2019.11.104

CellPress

Cell Reports
Article

Mutual Zonated Interactions of Wnt and Hh Signaling Are Orchestrating the Metabolism of the Adult Liver in Mice and Human

Erik Kolbe,[1] Susanne Aleithe,[2] Christiane Rennert,[1,10] Luise Spormann,[1] Fritzi Ott,[1] David Meierhofer,[3] Robert Gajowski,[3] Claus Stöpel,[4] Stefan Hoehme,[4] Michael Kücken,[5] Lutz Brusch,[5] Michael Seifert,[6] Witigo von Schoenfels,[7] Clemens Schafmayer,[7] Mario Brosch,[8] Ute Hofmann,[9] Georg Damm,[10] Daniel Seehofer,[10] Jochen Hampe,[8] Rolf Gebhardt,[1] and Madlen Matz-Soja[1,11,*]

[1]Rudolf-Schönheimer-Institute of Biochemistry, Faculty of Medicine, Leipzig University, Leipzig 04103, Germany
[2]Department of Neurology, Leipzig University, Leipzig 04103, Germany
[3]Max Planck Institute for Molecular Genetics, Mass Spectrometry Faculty, Berlin 14195, Germany
[4]Institute for Computer Science, Leipzig University, Leipzig 04103, Germany
[5]Center for Information Services and High Performance Computing, Technische Universität Dresden, Dresden 01069, Germany
[6]Institute for Medical Informatics and Biometry, Carl Gustav Carus Faculty of Medicine, Technische Universität Dresden, Dresden 01307, Germany
[7]Department of General Surgery and Thoracic Surgery, University Hospital Schleswig-Holstein, Kiel 24105, Germany
[8]Medical Department 1, University Hospital Dresden, Technical University Dresden, Dresden 01069, Germany
[9]Dr. Margarete Fischer-Bosch Institute of Clinical Pharmacology, University of Tübingen, Stuttgart 70376, Germany
[10]Department of Hepatobiliary Surgery and Visceral Transplantation, University Hospital, Leipzig University, Leipzig 04103, Germany
[11]Lead Contact
*Correspondence: madlen.matz@medizin.uni-leipzig.de
https://doi.org/10.1016/j.celrep.2019.11.104

SUMMARY

The Hedgehog (Hh) and Wnt/β-Catenin (Wnt) cascades are morphogen pathways whose pronounced influence on adult liver metabolism has been identified in recent years. How both pathways communicate and control liver metabolic functions are largely unknown. Detecting core components of Wnt and Hh signaling and mathematical modeling showed that both pathways in healthy liver act largely complementary to each other in the pericentral (Wnt) and the periportal zone (Hh) and communicate mainly by mutual repression. The Wnt/Hh module inversely controls the spatiotemporal operation of various liver metabolic pathways, as revealed by transcriptome, proteome, and metabolome analyses. Shifting the balance to Wnt (activation) or Hh (inhibition) causes pericentralization and periportalization of liver functions, respectively. Thus, homeostasis of the Wnt/Hh module is essential for maintaining proper liver metabolism and to avoid the development of certain metabolic diseases. With caution due to minor species-specific differences, these conclusions may hold for human liver as well.

INTRODUCTION

The liver simultaneously fulfills a multitude of metabolic tasks with partially opposing aims, such as synthesis and degradation of carbohydrates or lipids, which is a scenario that requires sophisticated orchestration by various mechanisms to satisfy the complex metabolic requirements of the organism. One of these is the spatial separation of functions along the sinusoids, resulting in remarkable metabolic heterogeneity of the hepatocytes. Based on their position within the liver lobules, roughly two zones can be distinguished, namely, a pericentral (pc) zone close to the central vein and a periportal (pp) zone located around the portal triads. The zones of protein expression for some metabolic functions like carbohydrate or xenobiotic metabolism are smooth, gradient-like, and flexible, varying due to changes in the oxygen, hormone, or nutrient levels (Gebhardt and Gaunitz, 1997; Kietzmann, 2017, 2019). Others like glutamine synthesis for ammonia detoxification are surprisingly static with steep gradients from one hepatocyte to another (Gebhardt and Mecke, 1983). Research during the last decade has shown that, in addition to the dynamic factors from blood, morphogenic pathways, such as the Wnt/β-catenin (Wnt), Hedgehog (Hh), members of the fibroblast growth factor (FGF) family, and many more, are deeply involved in regulating metabolism in the mature liver (Gebhardt and Matz-Soja, 2014).

Wnt and Hh signaling were originally known for their contribution in the developmental processes during embryogenesis and are expressed in adult hepatocytes next to non-parenchymal liver cells. Briefly, the Wnt pathway is triggered by the binding of Wnt ligands to the receptor machinery consisting of Frizzled (FZD) proteins and low-density lipoprotein-receptor-related protein (LRP5/6). Consequently, the cytosolic β-catenin (CTNNB1) destruction complex, set up by adenomatous polyposis coli (APC), axis inhibition protein (AXIN), glycogen synthase kinase-3-β (GSK3β), and casein kinase-1 (CK1), is inactivated. Thus, CTNNB1 is prevented from phosphorylation and subsequent proteasomal degradation. As a result, CTNNB1 accumulates in the cytoplasm, translocates to the nucleus, and binds to T cell factor/lymphoid enhancer factor (TCF/LEF), which causes regulation of the transcription of Wnt target genes (Figure S1) (Dai et al., 2019). Active Wnt signaling can be attenuated through negative

Wnt signaling pathway

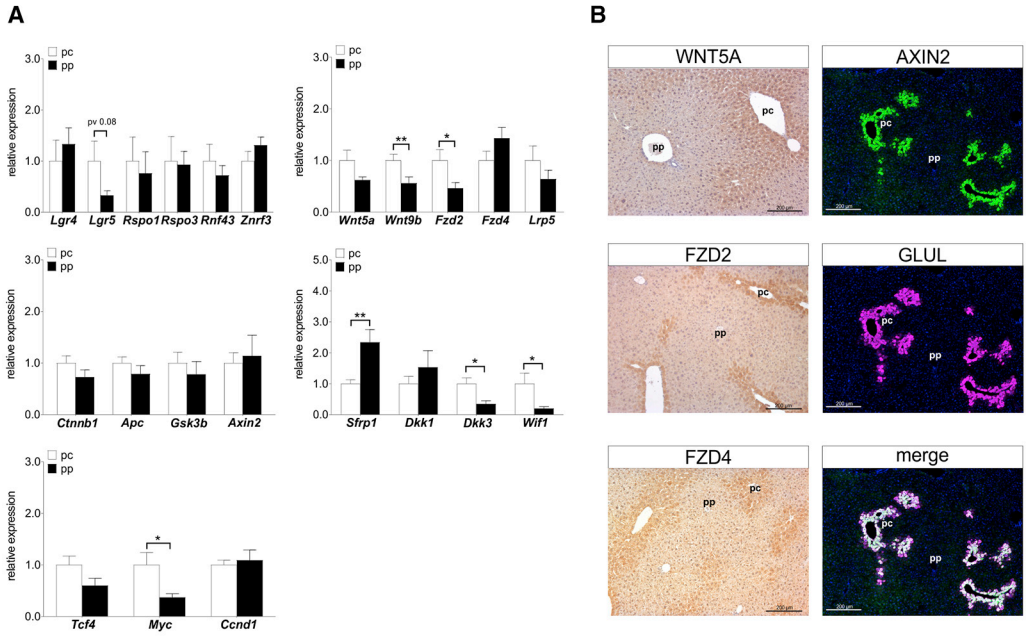

Hh signaling pathway

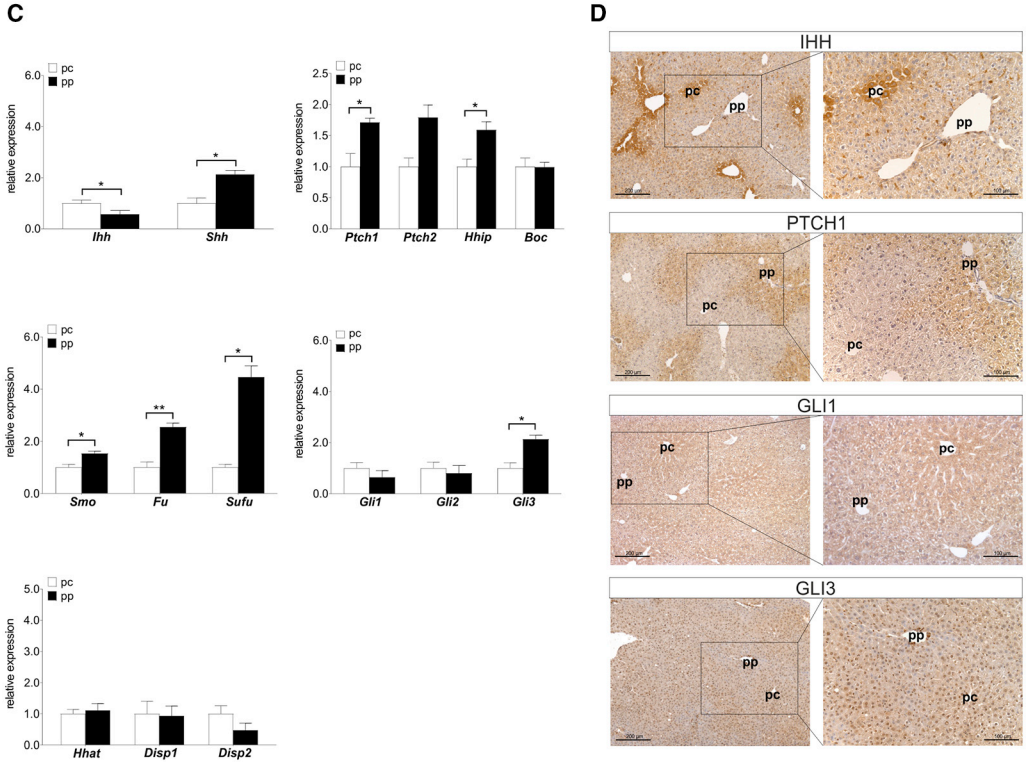

(legend on next page)

regulators, such as secreted SFRP1 and Wnt inhibitory factor 1 (WIF1) (Cruciat and Niehrs, 2013). Furthermore, Wnt signaling is controlled by the RSPO-LGR/RNF43-ZRNF3 module by clearance of FZD receptors (Rocha et al., 2015; Planas-Paz et al., 2016).

Hh signaling can be triggered by the binding of Hh ligands (e.g. Indian Hh [IHH] and Sonic Hh [SHH]) to the receptor Patched (PTCH). Ligand binding to PTCH leads to activation of the coreceptor Smoothened (SMO), which results in the release of the glioma-associated oncogene transcription factors (TFs) (GLI1–3) from the sequestering impact of suppressor of fused (SUFU). Finally, the GLI factors translocate to the nucleus and activate Hh-specific target genes (Figure S1) (Salaritabar et al., 2019).

Wnt signaling is required for the maintenance of the pc-based metabolic phenotype (e.g., synthesis and xenobiotic metabolism), whereas its inhibition causes a decrease in pc gene expression and a concomitant increase in pp markers (e.g., urea synthesis and β-oxidation) (Benhamouche et al., 2006; Burke and Tosh, 2006). Concerning the Hh pathway, it is known that inhibition of its activity in adult hepatocytes leads to a disturbed IGF1 (insulin-like growth factor) axis (Matz-Soja et al., 2014) and, in mutual interaction with the liver circadian clock, to steatosis (Matz-Soja et al., 2016; Marbach-Breitrück et al., 2019). It is known that both pathways considerably interact during development (Kalderon, 2002; Song et al., 2015; Noubissi et al., 2018) as well as in the adult stage in other organs (e.g., intestine [van den Brink et al., 2004]). Therefore, we hypothesized that both pathways also interact in the adult healthy liver and especially within hepatocytes and, thus, orchestrate liver zonation in close cooperation. Indeed, initial work *in vitro* showed that the TFs of the Hh cascade positively influence the transcription of several Wnt genes, such as Wnt5a (Wingless-type MMTV integration site family, member 5a) and Dkk1 (Dickkopf1) (Schmidt-Heck et al., 2015).

In the present work, we have investigated side by side (1) the spatial cellular distribution of key compartments of the Wnt and the Hh signaling and (2) the molecular interactions of both pathways in hepatocytes from normal and transgenic mice with altered or impaired activit. Furthermore, we have studied the metabolic consequences of these alterations using various OMICs techniques (transcriptome, proteome, and metabolome). Based on these data, a mathematical model was developed that provides the first insights into the mechanistic connection of the two pathways. The results of this study highlight the interconnections of Wnt/Hh signaling in shaping zonation of the adult liver and their fundamental relevance for the control of liver metabolism.

RESULTS

Wnt and Hh Are Heterogeneously Distributed in the Liver Parenchyma

To study the localization of the Wnt/Hh pathways, we analyzed the expression of selected core pathway genes in isolated hepatocytes from the pp and pc zones of C57BL6/N mice. Concerning the Wnt controlling the RSPO-LGR4/5-ZNRF3/RNF43 module, we could confirm dominant expression of *Lgr5*, *Rspo1/3*, and *Rnf4* in the pc hepatocytes compared with that in the pp ones (Planas-Paz et al., 2016). However, *Lgr4* and *Znrf3* showed a trend to be more greatly expressed in the pp area (Figure 1A). The expression of *Wnt5a* and *Wnt9b* was lower in the pp area, which was also indicated by immunohistochemistry (IHC) for the WNT5A protein (Figure 1B). Similar gene expression and protein translation along the pc zone could be observed for *Fzd2.* Likewise, the FZD4 protein showed a predominant staining in the pc zone. In the case of the genes encoding so-called "destruction complex" proteins, we detected only slight upregulation of *Ctnnb1*, *Gsk3β* and *Apc* in the pc zone but no differences in the expression of *Axin2* (Figure 1A). In contrast, AXIN2 was strongly zonated in the first two layers of hepatocytes around the central vein that nicely corresponds to GLUL protein localization (Figure 1B). As already published by several groups, the CTNNB1 protein could be detected in the pc zone (data not shown) (Benhamouche et al., 2006; Yang et al., 2014). For the mRNA of the negative regulator genes of Wnt signaling, we observed a pp predominance of *Sfrp1* and *Dkk1*, as well as a pc preference for *Dkk3* and *Wif1* (Figure 1A). In the case of Wnt TF *Tcf4* and transcriptional target *Myc*, the gene expression was stronger in the pc hepatocytes, whereas *Ccnd1* showed equal results.

Next, we asked how the Hh signaling components are localized in the liver parenchyma. Concerning the Hh ligand *Ihh*, the results clearly confirmed the already published pc zonation (Gebhardt and Matz-Soja, 2014) (Figure 1C) but further showed a strong colocalization with the Wnt-regulated proteins GLUL and AXIN2 (Figure 1D). Interestingly, all other Hh-signaling-associated genes with significant spatial preference showed a much stronger expression in hepatocytes from the pp zone (Figure 1C). In detail, we observed strong upregulation of the ligand *Shh* and the receptors *Ptch1* and *Ptch2* (Figure 1C). In the case of PTCH1, the pp localization was also confirmed by IHC (Figure 1D). Additionally, the coreceptor *Smo* showed distinct higher expression in the pp hepatocytes, which is also true for the negative regulators *Sufu* and *Fu*. In the case of the TF of Hh signaling, only *Gli3* showed significantly higher expression in the pp zone, whereas *Gli1* and *Gli2* exhibited no zonal division (Figure 1C). Interestingly, staining of the GLI proteins displayed predominant staining in the cytoplasm in pc hepatocytes for GLI1 and GLI3 with a clear nuclear staining in the case of GLI3 (Figure 1D), whereas GLI2 was not detectable (data not shown). The Hh-ligand-palmitoylating enzyme *Hhat,* as well as *Disp1* and *Disp2*, responsible for long-range Hh secretion, were found to have no significant zonal preference (Figure 1C).

Regarding the zonation of Wnt signaling in humans, we were able to detect CTNNB1 and LGR5 in human samples whereby CTNNB1 shows congruent results to the pc localization in

Figure 1. Lobular Distribution of Wnt/Hh Gene and Protein Expression in C57BL6/N Mice

(A) qPCR of Wnt pathway genes in isolated pp and pc hepatocytes from male C57BL6/N mice (n = 5–9). Data represented as mean ± SEM.

(B) IHC and IFC of Wnt protein expression in male C57BL6/N liver sections.

(C) qPCR of Hh genes in isolated pp and pc hepatocytes from male C57BL6/N mice (n = 4–11). Data represented as mean ± SEM.

(D) IHC of Hh pathway proteins in male C57BL/N liver sections.

See also Figure S1.

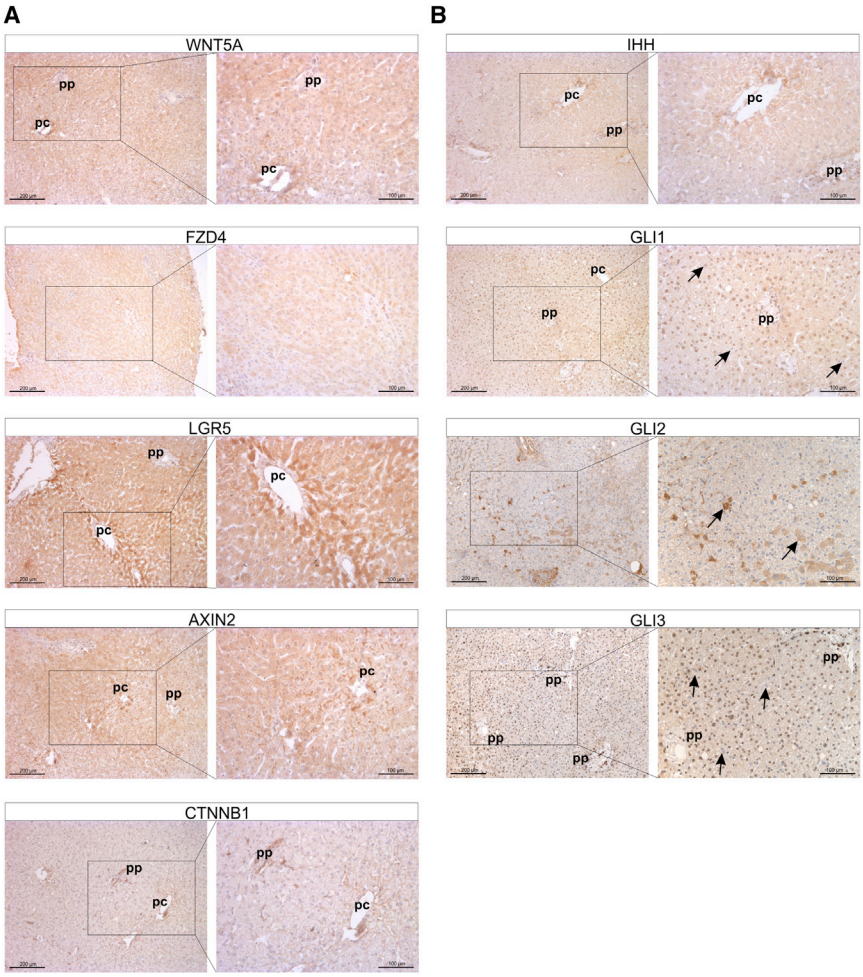

Figure 2. Lobular Distribution of Wnt/Hh Pathway Protein Expression in Humans

(A) IHC of Wnt proteins WNT5A, FZD4, LGR5, AXIN2, and CTNNB1 on human liver biopsy slides. (B) IHC of and Hh pathway proteins IHH, GLI1, GLI2, and GLI3 on human liver biopsy slides. See also Table S1.

C57BL6/N mice (Figure 2A). Inconsistent with the murine situation, the Wnt receptor FZD4 shows a scattered distribution spanning the whole parenchyma (Figures 1B and 2A). Also, human WNT5A and AXIN2 localization diverges from the murine-distinct pc zonation. Looking at the Hh-related proteins, we were able to depict a pc localization of the ligand IHH (Figure 2B). In addition, the GLI proteins could be visualized. GLI1 and GLI3 show a strong nuclear staining spanning the whole parenchyma, with the exception of single non-zonated cells with unstained nuclei (black arrows). In contrast, GLI2 is rather localized in the cytoplasm of single randomly distributed hepatocytes (black arrows, Figure 2B).

These results are confirmed by previous studies in which human samples of the pp and pc region were obtained by laser capture microdissection and analyzed for gene expression by RNA sequencing (Brosch et al., 2018). The results show that central genes of the Wnt pathway, such as AXIN2, LGR5, and RSPO3, are also present pc in humans, where negative regulators such as DKK3 are expressed pp (Table S1).

Activation of Wnt Leads to an Activation of the Hh Pathway

To investigate the consequences of hepatic Wnt pathway activation, the resulting impact on Hh signaling, and subsequent metabolic changes, we used Apc^{homo} mice, which carry a homozygous floxed exon 14 in the *Apc* allele (Shibata et al., 1997; Ueberham et al., 2015). In the RSPO-LGR4/5-ZNRF3/RNF43 module, the downregulation of the negative regulator *Apc* causes a significant decrease in *Lgr4* expression as well as a distinct reduction of *Rspo1* and *Rspo3* in isolated hepatocytes (Figure S2A). By contrast, *Lgr5, Rnf43*, and *Znrf3* showed significant upregulation, indicating a fine-tuned feedback mechanism of the downstream target genes of the RSPO-LGR4/5-ZNRF3/RNF43 module. Not less surprising due to *Apc* downregulation, there is a strong upregulation of the Wnt ligand and receptors *Wnt5a*, *Fzd4*, and *Lrp5,* indicating Wnt activation. However, the expression of *Wnt9b* and *Fzd2* is not affected due to Wnt activation (Figure S2A). IHC analyses revealed an enlargement of the WNT5A-, FZD2-, and FZD4-expressing pc area zone of Apc^{homo} mice (Figure S2B). Referring to the genes of the destruction complex, we confirmed the upregulation of *Axin2* due to downregulation of *Apc* by IHC (Colnot et al., 2004), whereas the expression of *Gsk3β* and *Ctnnb1* was not altered (Figures S2A and S2B). Furthermore, co-localized zonal expansion of AXIN2 with the GLUL protein was observed in Apc^{homo} mice (Figure S2C). A segmentation analysis of the expression shift of both proteins by using the *TiQuant* software (Friebel et al., 2015) indeed confirmed this co-localized enlargement by pixel quantification, with an almost identical increase in the GLUL-stained area (5.6-fold) with the AXIN2 stained area (5.7-fold) (Figure S2D). However, the analysis also revealed a significantly larger GLUL-stained area overlapping AXIN2 staining (GLUL-AXIN2) due to Wnt activation. Considering the extracellular antagonists of the Wnt signaling, a strong downregulation of *Sfrp1* as well as a reduction of *Dkk3* and *Wif1* was observed, whereas *Dkk1* showed no changes. Additionally, the obvious expression increase in the TF *Tcf4* and *Myc,* as well as the slight downregulation of *Ccnd1*, reflected the upregulation of the canonical Wnt activity (Figure S2A).

To investigate the feedback of Wnt on the Hh pathway in hepatocytes, we first analyzed the expression and protein translation of several Hh components in the Apc^{homo} mice. Considering the ligands *Ihh* and *Shh*, only the expression of *Ihh* was affected by

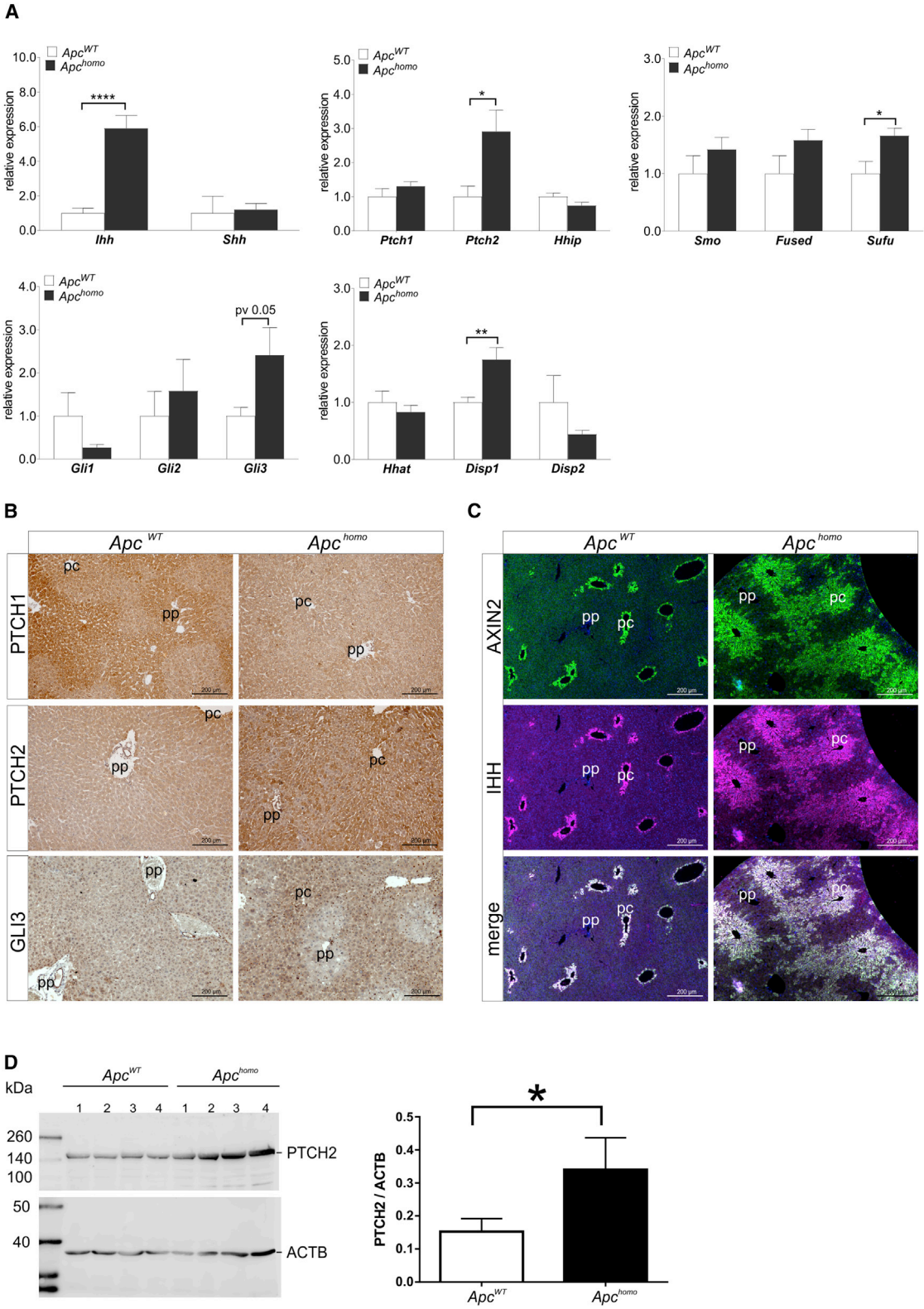

Figure 3. Influence of APC Reduction on Hh Signaling Expression and Zonation

(A) qPCR of Wnt gene expression in isolated hepatocytes from Apc^{WT} (n = 5–9) and Apc^{homo} (n = 5–9) mice. Data represented as mean ± SEM.

(B) IHC of Hh proteins PTCH1, PTCH2, and GLI3 on Apc^{WT} and Apc^{homo} mice liver.

(legend continued on next page)

the activation of Wnt signaling, as confirmed by IHC (Figures 3A and 3C). On the protein level, IHH and AXIN2 showed distinct colocalized expression in Apc^{WT} that was strongly expanded in Apc^{homo} mice, indicating the direct dependency of IHH on Wnt activity in single hepatocytes (Figure 3C).

Analyzing Hh receptors PTCH1/2 by IHC, we observed a contrary impact of Wnt activation in which PTCH1 pp expression was lost, whereas PTCH2 expression was scattered over the whole parenchyma (Figure 3B). The loss of *Ptch1* was not detectable by qPCR, whereas significant upregulation of *Ptch2* was observed in Apc^{homo} mice (Figure 3A). The upregulation of *Ptch2* was also confirmed by a significant increase in the protein level by western blot analysis in isolated hepatocytes of the *Apc* mice (Figure 3D). Due to *Apc* downregulation, we also found an upregulation of *Smo*, *Fu*, and *Sufu* (Figure 3A). Among the Hh TFs, the expression of proteins that could form a repressor, namely, *Gli2* and *Gli3,* were positively affected due to the upregulation of the Wnt signaling, whereas *Gli1* showed lower expression (Figure 3A). By performing GLI3 IHC, we revealed that not only the amount of the protein increases but also the expansion of the GLI3-positive cells followed a strong gradient around the pc area in the Apc^{homo} mice. However, in the Apc^{WT} mice, no pronounced zonation of the protein could be detected (Figure 3B). Among prominent genes encoding proteins essential for Hh secretion, we found a significant upregulation of *Disp1* and a slight downregulation of *Disp2*, whereas the expression of *Hhat* was not affected in the Apc^{homo} mice (Figure 3A).

Deletion of Hh Signaling Triggers Transcriptional Expression of Wnt Pathway

To address the question of how alteration of hepatic Hh signaling can change the Wnt cascade, we used transgenic SAC mice with parenchymal-specific Hh inhibition by the deletion of the coreceptor *Smo* (Matz-Soja et al., 2014). A global view of the individual Hh signaling genes showed that the deletion of *Smo in vivo* leads to decreased expression of *Ihh* and *Shh*, as well as that of the TF *Gli1* and *Gli3* (Figure S3). Regarding the expression of Hh negative feedback molecules, *Ptch1* was increased and *Hhip1* was downregulated, whereas *Fu* and *Sufu* were not affected. *Hhat* was strongly upregulated, wehreas *Disp2* showed a slight decrease (Figure S3).

Concerning Wnt signaling, the deletion of *Smo* resulted in a strong upregulation of the RSPO-LGR4/5-ZNRF3/RNF43 module (Figure 4A). Furthermore, the expression of *Wnt5a*, *Fzd4*, *Fzd2*, and *Lrp5* was increased, whereas *Wnt9b* displayed no change (Figure 4A).

This increase in gene expression was not accompanied by an expansion of the protein expression zone in IHC for WNT5A, FZD4, and FZD2, as observed in Apc^{homo} mice. The zonal spreading was rather identical between SAC-knockout (KO) and SAC-wild-type (WT) mice (Figure 4B), indicating that Hh signaling does not control the spatial expression of Wnt signaling and that the mechanisms are subject to very distinct and fine-tuned regulation. This is especially visible in the expression of *Axin2*, which is significantly upregulated in isolated hepatocytes of SAC-KO mice, whereas no significant increase in the number of AXIN2- and GLUL-expressing hepatocytes could be visualized by immunofluorescence (IF) (Figure 4C). However, concerning the segmentation analysis of the individual protein distribution, the GLUL-positive zone harbored a markedly lower number of AXIN2-positive hepatocytes in the SAC-KO than that in the SAC-WT mice (GLUL-AXIN2) (Figure 4D). Conversely, a significant increase was found in AXIN2-positive hepatocytes outside the GLUL-positive zone (AXIN2-GLUL) (Figure 4D), a finding that is in line with the upregulation of *Axin2* at the mRNA level. However, the IHC of CTNNB1 indicated no stronger Wnt activity because it displayed no increase in nuclear staining (data not shown), although the expression of the *Ctnnb1* gene was significantly increased in hepatocytes from SAC-KO mice (Figure 4A). Interestingly, genes encoding proteins for the negative regulators of Wnt signaling, such as *Sfrp1*, *Dkk3*, and *Wif1*, were upregulated, whereas *Dkk1* was not affected. Correspondingly, no change was found in the expression of *Tcf4* due to *Smo* deletion (Figure 4A).

Mathematical Model for Wnt/Hh Crosstalk and Spatial Patterning

Given the large complementary localization of Wnt and Hh pathways and their mutual interaction, we asked whether the complexity could be reduced by a mathematical model. The experimental base for constructing this model were the results mentioned above and further gene expression analyses of Wnt- and Hh-related genes after *in vitro* small interfering RNA (siRNA) knock down of several Wnt/Hh pathway targets (Figure S4A). From the *in vitro* knockdown data, a condition-dependency network was constructed depicting the relations of Wnt and Hh genes in response to the siRNA knockdowns (Figure S4B).

To analyze how the response of each gene to the knockdown is correlated to every other gene, a clustered correlation matrix was constructed (Figure 5A). The heatmap depicts the choice of gene activation versus inhibition along with hierarchical clustering analysis of correlation coefficients. We observed that some core Hh genes (*Smo*, *Ihh*, *Shh*, *Fu*, and *Gli3*) are strongly correlated with each other and grouped into one cluster. The same does not appear to be true for the Wnt pathway genes (Figure 5A). In line with our observation in the Apc^{homo} mice, *Ptch1* and *Ptch2* behave differently and were clustered far away within the correlation tree (Figures 3B and 5A).

From the cumulative *in vivo* and *in vitro* data, the model was constructed to simulate the spatial interactions of Wnt and Hh within the liver lobule (Figure 5B). We used the following assumptions in the model: Wnt ligands are secreted throughout the computational domain but predominantly by the central vein and diffuse. Wnt ligands activate the intracellular Wnt components and are counteracted by APC. Furthermore, the analysis revealed that the Wnt ligands *Wnt5a* and *Wnt9b* are both

(C) IF double staining of Wnt target protein AXIN2 and Hh ligand IHH on Apc^{WT} and Apc^{homo} mice liver sections.
(D) PTCH2 immunoblot analysis of isolated hepatocytes from Apc^{WT} (n = 4) and Apc^{homo} (n = 4) mice (left). β-Actin (ACTB) was used as loading control. Data represented as mean ± SEM.
See also Figure S2.

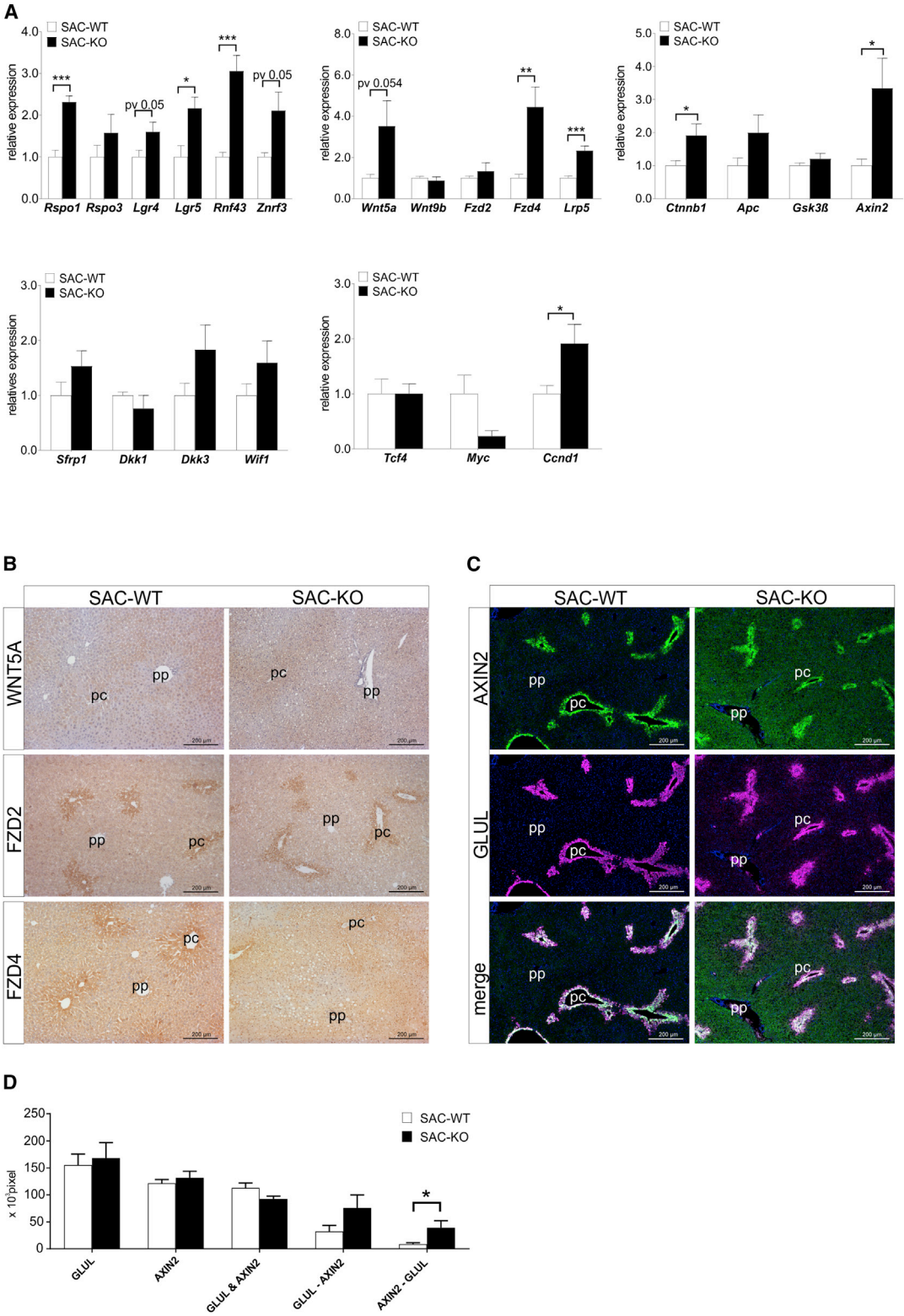

Figure 4. Deletion of Hepatic SMO Lead to Local Activation of Wnt Pathway

(A) qPCR of Wnt gene expression in isolated hepatocytes from SAC-WT (n = 3–7) and SAC-KO (n = 4–7) mice. Data represented as mean ± SEM.

(B) IF double staining of Wnt targets AXIN2 and GLUL on SAC-WT and SAC-KO mice liver sections.

(legend continued on next page)

negatively correlated with *Shh*, whereas the intracellular components of the Wnt pathway showed no obvious correlation pattern (Figure 5A). Supported by these anti-correlated responses of *Wnt5a*, *Wnt9b*, and *Shh* and the lack of spatial co-localization between the Wnt ligands and SHH, we assume that the maximum possible intracellular Wnt pathway activity is decreased by the presence of SHH.

Moreover, we make the simple assumption in the model that Wnt ligands suppress SHH expression. From the concomitant reduction of *Shh* by *Smo* deletion, we assume that SHH is activated by SMO and diffuses. IHH is activated by both SMO and the intracellular Wnt pathway components (Figure 5A). The latter assumption is inferred by the observed expression patterns (Figure S4A). Finally, from the unidirectional expression of GLI3 and IHH in our animal models and the positive correlation of GLI3 and SHH in the gene to knockdown the response matrix (Figure 5A), we assume GLI3 activation by both IHH and SHH.

The control, Apc^{homo}, SAC-KO, and combined Apc^{homo}/SAC-KO cases are depicted in Figure 5B. Each panel represents the same tissue domain, chosen slightly larger than a single liver lobule shown in the middle of the 2D cross section. The simulation results for individual model components are displayed as color-coded concentration fields: white for zero concentration and more saturated color for higher concentrations. In all cases, there were higher concentrations of Wnt pc and SHH pp. Crucial for this pattern was the increased production of Wnt pc and inhibition of SHH by Wnt. The intracellular components of the Wnt pathway were also strongest pc, the expression zone expanded upon decreasing APC, and their peak expression increased in SAC-KO (compare with Figures 4 and S2). IHH showed a pattern similar to the intracellular Wnt components but was decreased in the SAC-KO case, in contrast to the intracellular Wnt components that were increased in the SAC-KO case. GLI3 was expressed more pp in the control and more pc in the Apc^{homo} case (compare with Figures 4 and S2).

By invoking the changes in Apc^{homo} and SAC-KO simultaneously, we can simulate a combined Apc^{homo}/SAC-KO case (see Figure 5B). We obtained an increased expression zone of the intracellular Wnt components and IHH similar to the Apc^{homo} scenario and changes in expression levels with similar quantity as the SAC-KO case.

The model can also account for the expression patterns of Wnt and Hh pathway components that have been observed in humans (Figure 2). To reproduce these patterns, we can use the same model structure as that developed for the mouse and only change a few parameter values, corresponding to quantitative differences of rate constants and/or expression levels between both species. In fact, it turns out that changing the paramaters in the equation for Wnt only (slower diffusion, increased uniform production, and increased degradation rates) is sufficient to qualitatively reproduce the observed patterns (Figure 5B). The simulations then correctly reproduce both characteristic differences: a larger background concentration of Wnt and a smaller zone around the central vein with further increased Wnt (Figure 5B). The predicted patterns of IHH and Wnt components are similar as those in mice, and Gli3 expression is almost constant. All these simulation results correspond very well to the observed patterns in Figure 2 and, where not measured yet, represent additional testable model predictions.

Metabolic Consequence of the Modulation of Wnt and Hh Signaling in the Liver

To explore the influence of Wnt/Hh signaling on hepatic metabolism, isolated hepatocytes of the transgenic as well as separated pp and pc cells from C57BL6/N mice were cultivated up to 24 h. After hepatocyte cultivation, the supernatant was used to determine the extracellular metabolite status by liquid chromatography-mass spectrometry (LC-MS). The obtained data were evaluated using MetaboAnalyst software (Chong and Xia, 2018). In general, principal-component analysis (PCA) showed clear separation between the WT and KO samples from the *Apc* and SAC mice, as well as between the pp and pc fractions, indicating distinct differences in the extracellular metabolites in the opposing groups (data not shown).

An initial global examination of the data showed a different pattern of changes in amino acid (aa) concentrations in cultures of pp and pc hepatocytes (Figure 4A). After deleting Smo in SAC-KO mice, the enriched metabolite sets resemble those of hepatocytes in the pp area, whereas activation of the Wnt pathway leads to a more pc-like metabolite set enrichment (Figure S5A). For instance, a broad set of aas (e.g., glutamine, histidine, tyrosine, tryptophan, and serine) showed lower abundance in the supernatant of pp cells compared with that in pc cells, which can also be detected for SAC-KO compared with SAC-WT hepatocytes. In contrast, the Apc^{homo} hepatocyte supernatant showed a pc-like metabolic signature. Quantitative metabolite enrichment analysis revealed a large set of metabolic liver functions that were zonated, including well-known zonated metabolic pathways, such as the urea cycle, glutamate metabolism, glycolysis, and aa metabolism, and many of them showed significant changes between the WT and KO samples of both tramsgenic mouse models, corresponding to the changes between pp and pc hepatocytes (Figure S5B). For example, the urea cycle was significantly upregulated in hepatocytes from the pp area as well as in the SAC-KO mice, whereas no change was measured in Apc^{homo} mice, a finding that was also true for glutamate metabolism.

Regarding the urea cycle, the hepatocytes from the Apc^{homo} mice consumed a lower concentration of arginine that was also true for the hepatocytes derived from the pc area (Figure 6A). By contrast, the hepatocytes from the SAC-KO mice displayed a much higher consumption of arginine than the SAC-WT mice, indicating a more pp behavior. The deletion of the Hh signaling also caused a significant increase in the ornithine concentration in the culture medium compared with that in the SAC-WT, a trend

(C) IHC of Wnt proteins CTNNB1, FZD2, FZD4, and WNT5A on SAC-WT and SAC-KO mice liver slides.
(D) Quantification of AXIN2/GLUL double staining on SAC-WT (n = 3) and SAC-KO (n = 4) mice liver sections by TiQuant software. The different segmentations in brief: positive-stained area (GLUL WT/KO; AXIN2 WT/KO), colocalized positive-stained area (GLUL and AXIN2 WT/KO), positive-stained GLUL area where AXIN2 is not detected (GLUL-AXIN2 WT/KO), and positive-stained AXIN2 area where GLUL is not detected (AXIN2-GLUL WT/KO). Data represented as mean ± SEM. See also Figure S3.

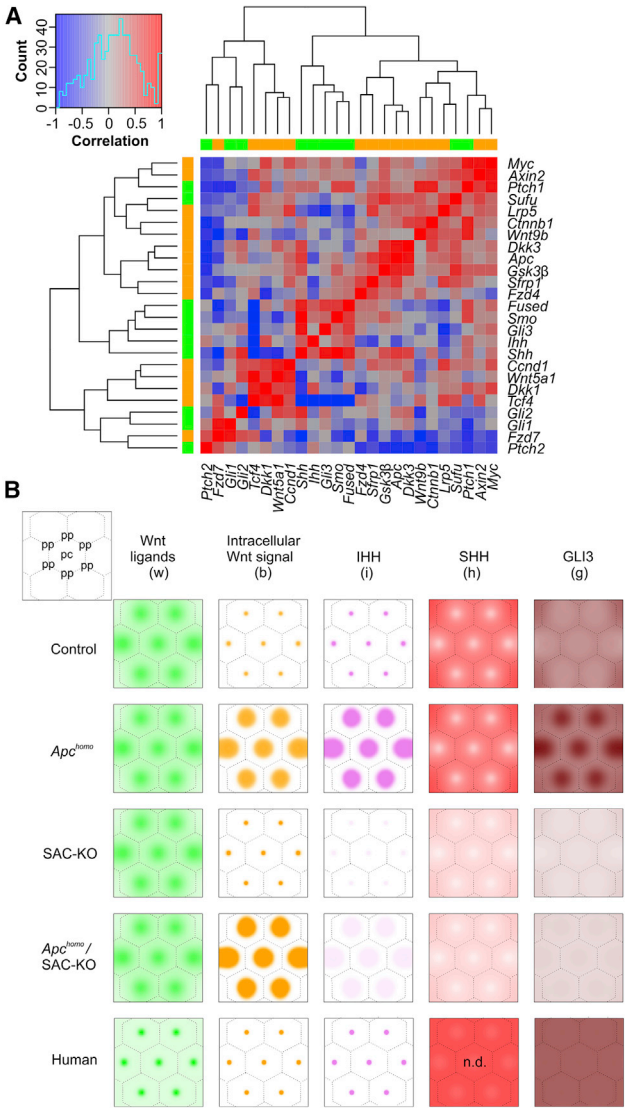

Figure 5. Results of the *In Vitro* Data Analysis and the Mathematical Model for Wnt/Hh Cross Talk and Spatial Patterning, See Also Figure S4

(A) Clustered correlation matrix showing pairwise correlations between measured gene expression levels for gene-specific expression responses to knockdowns (red: positive correlation, blue: negative correlation, gray: no correlation). Genes of the Hh pathway are marked in green and genes of the Wnt pathway are marked in orange.

(B) Results of the mathematical model for the Control, Apc^{homo}, SAC-KO, and combined Apc^{homo} /SAC-KO and human conditions. White corresponds to zero concentration, and increasing color saturation refers to higher concentrations. Five panels in each row show the spatial concentration fields, obtained simultaneously at steady state, for Wnt ligand (w), intracellular Wnt pathway activity (b), IHH ligand (i), SHH ligand (h), and GLI3 (g). Different colors serve to distinguish individual rows. The spatial domain is chosen to cover one hexagonal lobule in the center surrounded by parts of adjacent 6 lobules. See also Figure S4.

that was also found in the supernatant of the pp cells compared with that in the pc cells (Figure 6A). The final amount of secreted urea was, as expected, considerably smaller in the supernatant of hepatocytes from Apc^{homo} mice than that seen in the pc cells. The higher amount of urea in the supernatant of the SAC-KO hepatocytes confirmed the periportalization of the cultured hepatocytes (Figure 6A).

To investigate the underlying mechanism of this observation, we performed shotgun proteomics analysis of liver material from the transgenic mice and analyzed the data using Ingenuity Pathway Analysis (IPA) software (Krämer et al., 2014). The results showed that the activation of the Wnt pathway led to a significant downregulation of core proteins in the urea cycle (e.g., ASL, ARG1, and ASS1), leading to the prediction of the downregulation of the whole pathway. By contrast, the prediction of the upregulation of the urea cycle in the SAC-KO mice resulted from the strong upregulation of CPS1 and the OTC enzyme (Figure 6A; Table S2). Although not a part of the urea cycle, glutaminase is an important enzyme for pp nitrogen metabolism that is predicted to be upregulated in SAC-KO mice and downregulated in Apc^{homo} mice.

Additionally, the catabolism of aas, which is predominantly localized in the pp area, was strongly upregulated in hepatocytes from SAC-KO mice (e.g., consumption of histidine, glutamine, serine, and tyrosine), whereas mice with activated Wnt signaling showed a downregulation of these aas (Figure 6B). These results were also confirmed by the IPA network analysis of SAC-KO mice that showed upregulation of enzymes involved in serine catabolism, (e.g., serine dehydratase and serine hydroxymethyltransferase), glutamine catabolism (e.g., glutaminase and glutamic-oxaloacetic transaminase), and tryptophan catabolism (e.g., indolamin-2,3-dioxygenase and arylformamidase). On the other hand, for Apc^{homo} mice, the analysis revealed a downregulation or no change in the expression of those enzymes that were upregulated in SAC-KO mice (Figure 6B; Table S3).

Because space does not allow us to present all affected metabolic pathways in detail, another example from lipid metabolism shall demonstrate that the responses to Hh and Wnt modulation follow the same pattern. For instance, cholesterol transport in SAC-KO mice was downregulated, whereas it appeared upregulated by Wnt activation (Figure 6C; Table S4). In detail, proteins involved in lipoprotein formation and vesicular transport, such as APOA1, APOE, and CLU, were downregulated in SAC-KO mice but were upregulated in Apc^{homo} mice.

To find a mechanism behind the regulation of pp functions by Hh signaling, we first clarified the question about whether the ligand IHH, which is the only pc-located Hh component, is responsible for this observation. Therefore, we studied IHH and SHH gain-of-function as well as loss-of-function analyses *in vitro*. The results show that a 48-h incubation with the recombinant IHH (rec IHH) protein leads to an increase in almost all genes investigated, whereby cholesterol biosynthesis (*Hmgcr*, *Hmgcs*, and *Cyp7A1*) was particularly strong affected after 48 h (Figure S6A). In contrast, increasing Hh activity by recombinant SHH (rec. SHH) did not result in significant changes of the investigated genes. Solely, a trend for an increase of *Otc* and *Cps1* by rec. SHH can be observed (Figure S6A).

To carry out IHH and SHH loss-of-function analyses, RNA interference experiments were performed. The deletion of *Ihh* shows a strong downregulation of the investigated genes after an incubation period of 72 h, whereby, again, the cholesterol

A Urea cycle

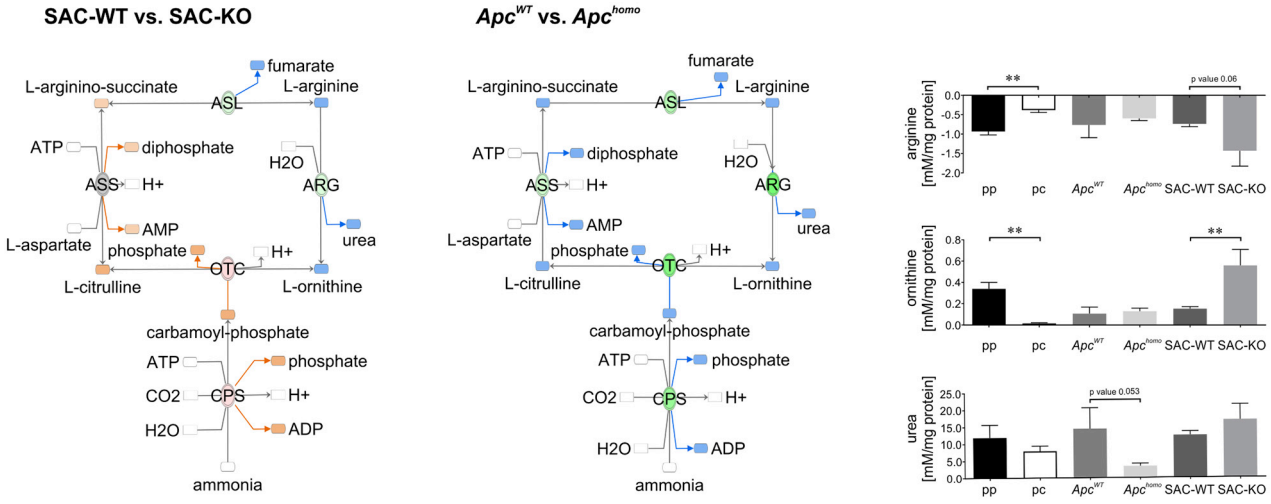

B Catabolism of amino acids

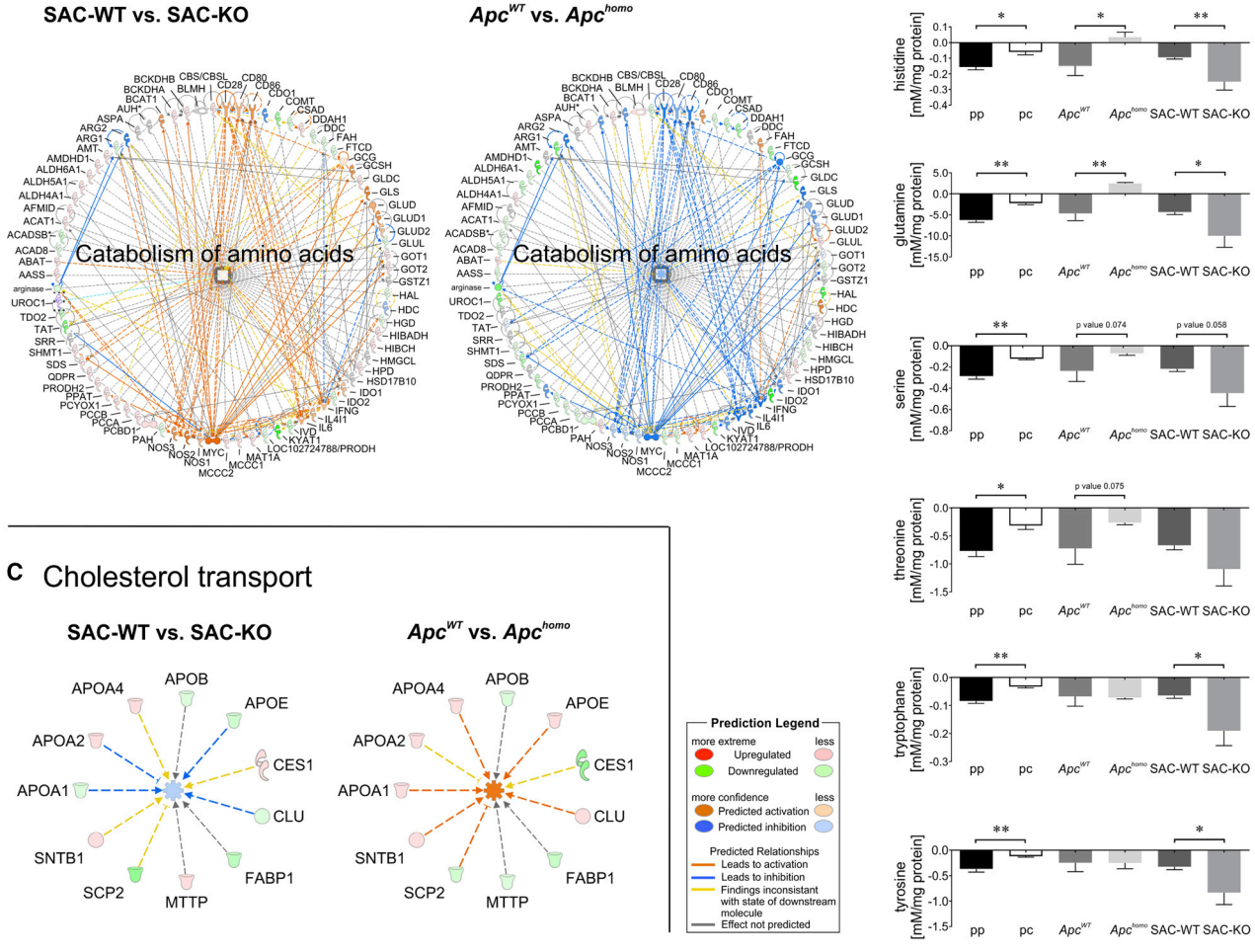

C Cholesterol transport

(legend on next page)

biosynthesis is mostly affected. In response to the deletion of *Shh*, no clear effects could be found due to mutual variations of the measured values (Figure S6B).

With regard to the function of IHH *in vivo*, we bred transgenic animals with hepatocyte-specific deletion of IHH and performed microarray analyses of liver tissue. To link the obtained data to pp-localized metabolic pathways, we searched the array for the studied *in vivo* genes, such as urea synthesis (*Cps*, *Arg1/1*, *Asl1*, *Ass1*, and *Otc*) and cholesterol metabolism (*Hmgcr/l/s*) (Figure S6C). The results suggest that IHH produced by the liver *in vivo* does not directly affect pp functions.

To show whether Hh signaling influences pp zonation by Gli TFs, we activated the Hh signaling pathway in hepatocytes of non-transgenic C57BL/6N mice *in vitro* by overexpression experiments (Figure S7). The cells were transfected individually with GLI1, GLI2, and GLI3 plasmid DNA, as well as in combination of all three TFs. The results of these analyses show that many of the genes examined react quite differently to the overexpression of the individual GLI factors. The genes of the urea metabolism (*Arg1*, *Otc*, and *Cps1*) show a decreased expression due to the overexpression of GLI1, whereas transfection with GLI2 and GLI3 lead to an increase of these genes compared to the mock control. The combination of all 3 TFs also shows an increase in the expression of the genes of the urea cycle, whereby the inhibitory effect of GLI1 is most likely masked by GLI2 and GLI3. In contrast, in the case of cholesterol metabolism, the overexpression of GLI1 seems to lead to an increase in the genes studied, which also applies to GLI2 and GLI3 (Figure S7).

DISCUSSION

The present study reveals insights into the regulation of metabolic liver zonation by the morphogen Wnt and Hh pathways, demonstrating their largely complementary lobular distribution and providing a paradigm for their mutual interplay in liver parenchyma. For the Wnt signaling, the known pc expression of core pathway components (Sekine et al., 2006; Braeuning and Schwarz, 2010; Preziosi et al., 2018) and of some members of the RSPO-LGR4/5-module (Planas-Paz et al., 2016), such as Rspo1/3, Lgr5, and Rnf4 could be confirmed, whereas other components like Lgr4 and Znrf3 tended to be more highly expressed pp. The most spectacular findings, however, concerned the impact of Wnt activity on the Hh cascade in adult hepatocytes, which had not been investigated before.

With respect to Hh signaling, we showed that the zonal distribution of its members, except IHH but including SHH and the Hh negative regulator *Sufu*, dominated in the pp area. Because SUFU is also known to be a negative regulator of Wnt signaling (Meng et al., 2001), its pp localization suggests a contribution to a pp Wnt antagonism. In contrast to other Hh pathway members, IHH is an exception and was expressed most distal from the portal vein, almost co-localized with AXIN2 (Figure 7). In accordance with the spatial separation between IHH and SHH, we found a highly elevated mRNA level of *Ihh* in conjunction with circular expansion around the central vein in Wnt-activated Apc^{homo} mice, whereas SHH did not respond. Interestingly, the negative regulators *Ptch2*, *Sufu*, and *Gli3* (potential repressor) were also upregulated *in vivo*. Thus, Wnt signaling seems to suppress pp Hh signaling but triggers the pc expression of IHH. This result may be a first indication that IHH has a completely different function in hepatocytes than is known from other tissues. Hh-ligand-secreting *Disp1* that is responsible for long-range Hh signaling (Caspary et al., 2002) is also increased by Wnt activation in Apc^{homo} mice, suggesting that IHH is formed as a secretory protein in the pc zone to transmit essential information from the liver to the periphery. This hypothesis is supported by the results of IHH modulation *in vivo*. The results show that a hepatocyte-specific deletion of IHH does not lead to a change in the pp functions studied, such as urea cycle and cholesterol metabolism. We interpret this result as a strong hint that liver-derived IHH signals to other (peripheral) organs, whereas liver pp metabolism is regulated by IHH from other sources, most probably the gut by the portal vein. The finding that IHH, but not SHH or DHH, travels by VLDL (Very low-density lipoprotein) in human blood (Queiroz et al., 2010) supports this hypothesis. In addition, we recently demonstrated that the IHH protein shows an oscillatory hepatic expression behavior that can also be detected in the serum of mice (Marbach-Breitrück et al., 2019).

The impact of Wnt signaling on the Hh pathway and vice versa was analyzed by mathematical modeling on the basis of the data obtained *in vivo* and *in vitro* from the Apc^{homo} and the SAC-KO mice. The model suggests that by assuming a steady gradient of WNT ligands from the central vein to the portal triad, the mutual negative correlation between SHH and WNT ligands is able to match the zonal distribution of Wnt and Hh activities in control and transgenic mice. Because IHH is activated by both SMO and intracellular Wnt pathway components, it is clear that the two Hh ligands play a different role in the liver even though both ligands positively influence GLI3. This reflects a dramatic change in a fundamental paradigm because so far it was thought that IHH would represent the hepatocellular activity of this pathway rather than SHH. In other organs, the manner in which both pathways

Figure 6. Alteration in Metabolic Zonation by Wnt/Hh Modulation

(A) IPA results for the urea cycle of proteome analysis data from liver material of Apc^{WT} (n = 5) versus Apc^{homo} (n = 6) and SAC-WT (n = 4) versus SAC-KO (n = 4) mice (left) and column representation of urea cycle metabolites in hepatocyte culture supernatants from Apc^{WT} (n = 3) versus Apc^{homo} (n = 5), SAC-WT (n = 5) versus SAC-KO (n = 3) mice and pp (n = 3) versus pc (n = 4) hepatocytes from C57BL6/N mice after 24-h incubation time (right). Normalization to total protein content was performed. Data represented as mean ± SEM.

(B) IPA results for aa degradation of proteome analysis data from liver material of Apc^{WT} (n = 5) versus Apc^{homo} (n = 6) and SAC-WT (n = 4) versus SAC-KO (n = 4) mice (left) and column representation of several aas in hepatocyte culture supernatant from Apc^{WT} (n = 3) versus Apc^{homo} (n = 5), SAC-WT (n = 5) versus SAC-KO (n = 3) mice and pp (n = 3) versus pc (n = 4) hepatocytes from C57BL6/N mice after 24-h incubation. (right). Normalization to total protein content was performed. Data represented as mean ± SEM.

(C) IPA results for cholesterol transport of proteome analysis data from liver material of Apc^{WT} (n = 5) versus Apc^{homo} (n = 6) and SAC-WT (n = 4) versus SAC-KO (n = 4) mice.

See also Figures S5, S6, and S7 and Tables S1–S6.

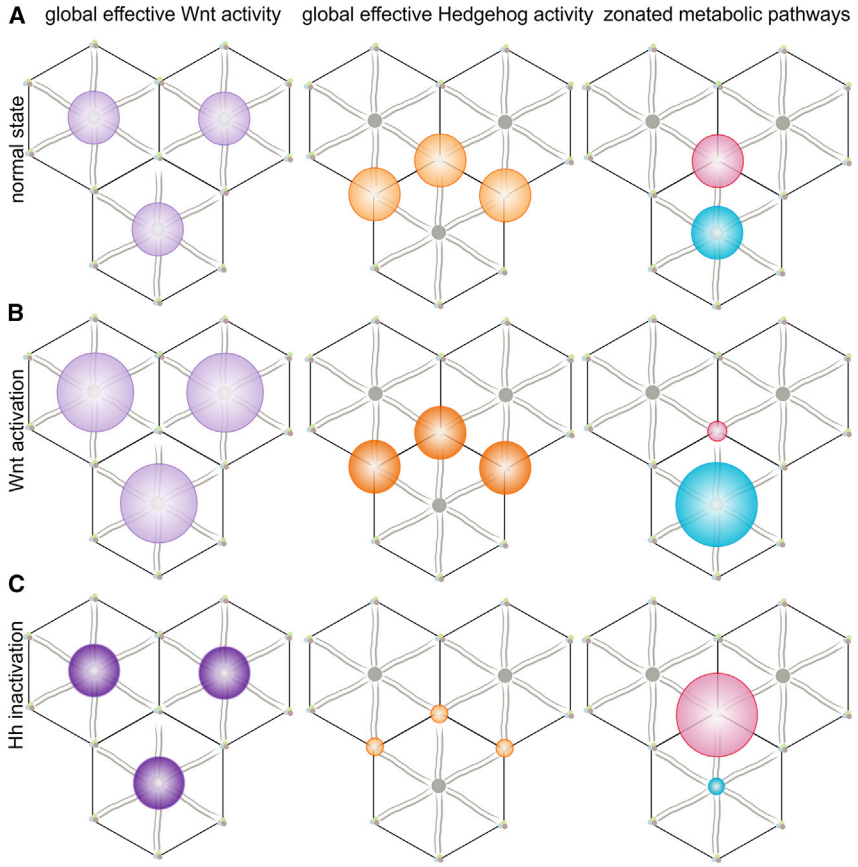

Figure 7. Interplay of Wnt and Hh Activity and Its Influence on Metabolically Zonated Pathways

(A) The Wnt (violet circle) and the Hh pathway (orange circle) in the normal state. Most of the Wnt-associated members are zonated in the pc area, whereas central Hh members are located in the pp area. The metabolically zonated pathway are in balance (blue circle represents pc localizated metabolic functions; pink circle represents pc localized metabolic functions).

(B) The activation of pc Wnt activity by *Apc* downregulation leads to a locally increase in Hh activity. The pc-zonated metabolic pathways become overrepresented, whereas the pp program is decreased.

(C) The inhibition of the pp-localized Hh leads to a locally limited increase in Wnt activity. The pp-zonated metabolic pathways become overrepresented, whereas the pc program is decreased.

communicate is controversial. In the adult gut, both pathways interact in an antagonistic way in which Gli1 inhibits Wnt signaling at a level below β-catenin phosphorylation (van den Brink et al., 2004). One potential protein that acts as an interface between the two pathways in most tissues is the soluble modulator SFRP1, which is known to antagonize Wnt signaling (Planas-Paz et al., 2016; Ding and Wang, 2017). However, our results indicate a more subordinate role of SFRP1 in the interplay of both pathways in hepatocytes. In SAC-KO mice, the expression of *Sfrp1* shows an upregulated trend but is strongly downregulated by Wnt activation in Apc^{homo} mice. Other proteins that serve as an intersection between the two pathways, such as GSK3β, CTNNB1, GLI1, and GLI3R, have been described (Song et al., 2015). In dorso-ventral patterning, Wnt antagonizes Hh signaling through the expression of the GLI repressor GLIR (Alvarez-Medina et al., 2008; Ulloa and Martí, 2010). However, all the described interaction concepts known for different types of cancer fail to explain the interaction of Wnt and Hh in the healthy liver. Therefore, we support the theory that Wnt and Hh cross talk occurs in a tissue- and metabolic-specific manner, a result of integrated, context-dependent cellular responses (Sethi and Vidal-Puig, 2010). This intercellular concept has also been described for the intestinal epithelium (Katoh and Katoh, 2006).

In contrast to liver zonation of Wnt and Hh in rodents, the knowledge about the human situation is rather rudimentary. The cause is most likely the difficult acquisition of unaltered healthy human liver tissue and, as also indicated by our results, a partially different localization in humans than in mice. For example, WNT5A was expressed in the pc area in mice, whereas in humans, the localization occurs in the pp zone (Beljaars et al., 2017). Furthermore, Brosch et al. (2018) demonstrated pc zonation of *Axin2* by transcriptome analysis of laser microdissected pp and pc human hepatocytes, which was also shown in our data. Concerning human Hh signaling proteins, we found IHH to be located pc, as already demonstrated in mice (Gebhardt and Matz-Soja, 2014). In addition, we showed that TF GLI1 and GLI3 are expressed in the nuclei of human hepatocytes under normal conditions, whereas GLI2 expression was solely cytosolic in single randomly distributed cells. This demonstrates that the Hh pathway is also active in the adult human liver where it might contribute to metabolic liver homeostasis, as has already been proven in mice (Matz-Soja et al., 2016). Although the morphogen pathways make an immense contribution to maintaining liver homeostasis, particularly in humans (Verdelho Machado and Diehl, 2018; Li et al., 2019), considerable additional work is needed to specify this in detail. Because the mathematical model established in the context of this work for the interaction of the Hh and the Wnt pathway in the mouse can also reproduce the results in humans very well, this model can be used in such future investigations on the limited liver material of patients.

The interplay of Wnt and Hh signaling described above is of the utmost importance for the regulation of metabolic liver zonation, as demonstrated by combining global gene expression, proteome data, and metabolome data obtained from cultured hepatocytes of pp and pc origin or isolated from the transgenic mice with modulated Wnt and Hh signaling. The range of metabolic functions analyzed covered the entire spectrum of liver metabolism and comprised examples from carbohydrate, aa, and lipid metabolism but also bile acid synthesis, oxidative stress, and drug metabolism, just to name a few (Figure S5 shows 50 examples).

All of them were clustered according to their pp or pc prevalence. Further analyses revealed that most of them responded to changes in Hh and Wnt activity depending on whether they belonged to the pp and pc clusters, respectively. Thus, loss of Hh activity by Smo leads to a dominance of pp functions, whereas activation of Wnt by APC knockout enhances pc functions. Concerning modulation of the Wnt pathway, similar findings were already deduced from gene expression studies, mainly with respect to ammonia detoxification (Benhamouche et al., 2006; Sekine et al., 2006) but not supported by metabolic studies. In the case of Hh modulation, we recently demonstrated that a loss of Hh activity strongly affects lipid metabolism (represented by pp-localized steatosis) and shifts the zonation of PPAR (Peroxisome proliferator-activated receptor alpha) TFs to a more pp localization (Matz-Soja et al., 2016). Moreover, in SAC-KO mice the synthesis of IHH is lowered but remains its circadian rhythmic expression in a narrow pc zone (Marbach-Breitrück et al., 2019).

As illustrated by our mathematical model, both morphogen pathways indeed contribute differently the alterations in metabolic zonation. Impairment of Hh affects mainly the capacity of the respective metabolic function, i. e. upregulation of pp functions and downregulation of pc functions. In contrast, activation of Wnt affects not only the capacity, but also leads to a pronounced extension of the pc expression zone of respective enzymes, e. g. glutamine synthetase, and reduces pp localized functions. These different patterns illustrated in Figure 7 could also be corroborated by our proteome studies and IHC of selected enzymes. The complex interplay of Wnt and Hh signaling pathways in liver and its global impact on metabolic zonation calls for intensive studies of the molecular mechanisms involved. Regulation of gene expression via various TFs may be one of them. Although some detailed studies of selected cases have been reported (Werth et al., 2006; Schmidt-Heck et al., 2015), even major regulatory steps within the Wnt/Hh module remain enigmatic. One such example is the role of GLI factors and their regulation in hepatocytes. Although the *Gli3* mRNA is much more strongly expressed in the pp area of the liver lobuli (Figure 1C), the localization of the GLI3 protein seems to dominate in the pc area (Figure 1D) where it is strongly enhanced when Wnt signaling is activated (Figure 3B). This lead to the hypothesis that here the repressor form of the GLI3 protein is affected by Wnt activity, resulting in increased suppression of pp metabolic functions. In SAC-KO mice, where *Gli3* is almost lost (Matz-Soja et al., 2016), no repression may be active, thus, leading to the observed increase of pp functions. Unfortunately, this scenario cannot be easily reproduced *in vitro*. This demonstrates the complexity of the interplay of the GLI factors and the need for further investigation, which may show what a possible GLI code for the regulation of hepatic pp functions might look like.

Limitations of the Study and Conclusion

The aim of this study was to gain profound insight into the complex interactions of the Wnt and Hh signaling in healthy liver of mice and humans and to elucidate of how these pathways jointly regulate metabolic zonation of liver parenchyma. Collectively, our results are based on a side-by-side investigation of two major morphogen pathways together with the intensive use of transcriptomics, proteomics, and metabolomics to provide insight into structural features and regulation of metabolic zonation in healthy adult mouse and human liver. The main findings were (1) Wnt and Hh signaling dominate in distinct lobular regions (pc and pp, respectively) and closely interact with each other at various levels, mainly by mutual repression; (2) there is a change in the paradigm that Hh signaling in the liver is controlled by SHH rather than IHH, which might possibly act as an endocrine signal; (3) the Wnt/Hh module in the liver governs a huge number of pp and pc metabolic functions where Hh inhibition leads to a periportalization and Wnt activation results in strong pericentralization, including striking extension of the pc zone; and (4) both morphogen pathways seem to act similarly in human liver. However, certain differences in the zonal distribution of signaling components call for caution to simply transfer the findings to the human situation. Nonetheless, it is obvious that any modulation of the Wnt/Hh module may cause severe disturbance of liver metabolism in many of its facets.

The present study shows several limitations that should be considered when drawing conclusions. These include the following. (1) The non-inclusion of the non-parenchymal cell (NPC) fraction in the analyses performed. We are well aware that these cell populations significantly contribute to the complex network in the liver because they express (and possibly secrete) large amounts of both Wnt and Hh ligands (Machado and Diehl, 2016). Intensive further analyses, however, are needed before the NPC fraction can be integrated into our mathematical model. (II) Another limitation is the adequate interpretation of human data. Although we have used human liver samples with an NAFLD (non-alcoholic-liver disease) activity score (NAS) of 0–1, it is clear that they do not represent healthy individuals. It is currently impossible to fully estimate the influence of the individual lifestyle of patients and the medication they take on both morphogen signaling and liver metabolism. Perhaps the development and use of novel *in vitro* systems, such as *in vitro* organoids, may improve this situation.

STAR★METHODS

Detailed methods are provided in the online version of this paper and include the following:

- KEY RESOURCES TABLE
- LEAD CONTACT AND MATERIALS AVAILABILITY
- EXPERIMENTAL MODEL AND SUBJECT DETAILS
  - Human subjects
  - Murine subjects
- METHOD DETAILS
  - Maintenance of the mice and feeding
  - Isolation and cultivation of primary mouse hepatocytes
  - Isolation of primary periportal and pericentral mouse hepatocytes
  - RNA isolation and quantitative real-time PCR (qPCR)
  - RNA interference
  - GLI overexpression experiments
  - *In vitro* IHH and SHH gain off function analysis
  - Immunohistochemistry
  - TiQuant - Protein quantification
  - Western Blot

SUPPLEMENTAL INFORMATION

Supplemental Information can be found online at https://doi.org/10.1016/j.celrep.2019.11.104.

ACKNOWLEDGMENTS

We would like to thank Jan Böttger for his technical guidance, preliminary efforts, and establishing the *Apc*^{homo} mouse model in the lab. Gratitude is also expressed for the excellent technical assistence of Doris Mahn and Vivien Teßmar. Furthermore, we would like to thank Dr. Petra Hirrlinger, Köbrig, and Michelle-Jessica Jannicke from the Medizinisches Experimentelles Zentrum (Faculty of Medicine) for taking excellent care of the mice. This work was supported by the Federal Ministry of Education and Research (BMBF, Germany) within the research network Systems Medicine of the Liver (LiSyM) (grant numbers 031L0054, 031L0033, and 031L0037); the Virtual Liver Network (VLN) (grant numbers 0315735, 0315736, 0315755, and 0315775); and the Deutsche Forschungsgemeinschaft (DFG, Germany) (grants MA 6610/2-1 and MA 6610/4-1).

AUTHOR CONTRIBUTIONS

Experimental design: RG(Leipzig), M.M.-S., and E.K.; Performing experiments: E.K., S.A., L.S., F.O., and M.M.-S.; Data acquisition: D.M., RG (Berlin), and U.H.; Computational analysis: M.K., M.S., L.B., C.S., and S.H.; Resourcing and care of human material: C.R., W.v.S., C.S., M.B., G.D., D.S., and J.H.; Data analysis, interpretation, and figure generation: M.M.-S., E.K., and S.A., Manuscript writing, reviewing, and editing: E.K., M.M.-S., R.G. (Leipzig), M.K., and L.B.

DECLARATION OF INTERESTS

R.G. (Leipzig) is listed as inventor on a patent application filed by the University of Leipzig (WO 2013/110749A1, Therapeutic use of activators of zinc finger protein GLI3).

Received: July 11, 2019
Revised: October 14, 2019
Accepted: November 25, 2019
Published: December 24, 2019

REFERENCES

Achanta, R., Shaji, A., Smith, K., Lucchi, A., Fua, P., and Süsstrunk, S. (2012). SLIC superpixels compared to state-of-the-art superpixel methods. IEEE transactions on pattern analysis and machine intelligence *34*, 2274–2282.

Alvarez-Medina, R., Cayuso, J., Okubo, T., Takada, S., and Martí, E. (2008). Wnt canonical pathway restricts graded Shh/Gli patterning activity through the regulation of Gli3 expression. Development *135*, 237–247.

Beljaars, L., Daliri, S., Dijkhuizen, C., Poelstra, K., and Gosens, R. (2017). WNT-5A regulates TGF-β-related activities in liver fibrosis. Am. J. Physiol. Gastrointest. Liver Physiol. *312*, G219–G227.

Benhamouche, S., Decaens, T., Godard, C., Chambrey, R., Rickman, D.S., Moinard, C., Vasseur-Cognet, M., Kuo, C.J., Kahn, A., Perret, C., and Colnot, S. (2006). Apc tumor suppressor gene is the "zonation-keeper" of mouse liver. Dev. Cell *10*, 759–770.

Braeuning, A., and Schwarz, M. (2010). beta-Catenin as a multilayer modulator of zonal cytochrome P450 expression in mouse liver. Biol. Chem. *391*, 139–148.

Brosch, M., Kattler, K., Herrmann, A., von Schönfels, W., Nordström, K., Seehofer, D., Damm, G., Becker, T., Zeissig, S., Nehring, S., et al. (2018). Epigenomic map of human liver reveals principles of zonated morphogenic and metabolic control. Nat. Commun. *9*, 4150.

Burger, H.J., Gebhardt, R., Mayer, C., and Mecke, D. (1989). Different capacities for amino acid transport in periportal and perivenous hepatocytes isolated by digitonin/collagenase perfusion. Hepatology *9*, 22–28.

Burke, Z.D., and Tosh, D. (2006). The Wnt/β-catenin pathway: master regulator of liver zonation? BioEssays *28*, 1072–1077.

Caspary, T., García-García, M.J., Huangfu, D., Eggenschwiler, J.T., Wyler, M.R., Rakeman, A.S., Alcorn, H.L., and Anderson, K.V. (2002). Mouse Dispatched homolog1 is required for long-range, but not juxtacrine, Hh signaling. Curr. Biol. *12*, 1628–1632.

Chong, J., and Xia, J. (2018). MetaboAnalystR: an R package for flexible and reproducible analysis of metabolomics data. Bioinformatics *34*, 4313–4314.

Colnot, S., Decaens, T., Niwa-Kawakita, M., Godard, C., Hamard, G., Kahn, A., Giovannini, M., and Perret, C. (2004). Liver-targeted disruption of Apc in mice activates beta-catenin signaling and leads to hepatocellular carcinomas. Proc. Natl. Acad. Sci. USA *101*, 17216–17221.

Cox, J., and Mann, M. (2008). MaxQuant enables high peptide identification rates, individualized p.p.b.-range mass accuracies and proteome-wide protein quantification. Nature biotechnology *26*, 1367–1372.

Cruciat, C.-M., and Niehrs, C. (2013). Secreted and transmembrane wnt inhibitors and activators. Cold Spring Harb. Perspect. Biol. *5*, a015081.

Dai, B., Ma, Y., Yang, T., Fan, M., Yu, R., Su, Q., Wang, H., Liu, F., Yang, C., and Zhang, Y. (2019). Synergistic effect of berberine and HMQ1611 impairs cell proliferation and migration by regulating Wnt signaling pathway in hepatocellular carcinoma. Phytother. Res. *33*, 745–755.

Ding, M., and Wang, X. (2017). Antagonism between Hedgehog and Wnt signaling pathways regulates tumorigenicity. Oncol. Lett. *14*, 6327–6333.

Friebel, A., Neitsch, J., Johann, T., Hammad, S., Hengstler, J.G., Drasdo, D., and Hoehme, S. (2015). TiQuant: software for tissue analysis, quantification and surface reconstruction. Bioinformatics (Oxford, England) *31*, 3234–3236.

Gebhardt, R. (1998). Isolation of periportal and pericentral hepatocytes. In Cytochrome P450 protocols, E.A. Shephard and I.R. Phillips, eds. (Humana Press), pp. 319–328.

Gebhardt, R., and Gaunitz, F. (1997). Cell-cell interactions in the regulation of the expression of hepatic enzymes. Cell Biol. Toxicol. *13*, 263–273.

Gebhardt, R., and Matz-Soja, M. (2014). Liver zonation: Novel aspects of its regulation and its impact on homeostasis. World J. Gastroenterol. *20*, 8491–8504.

Gebhardt, R., and Mecke, D. (1983). Heterogeneous distribution of glutamine synthetase among rat liver parenchymal cells in situ and in primary culture. EMBO J. *2*, 567–570.

Gebhardt, R., Lerche, K.S., Götschel, F., Günther, R., Kolander, J., Teich, L., Zellmer, S., Hofmann, H.-J., Eger, K., Hecht, A., and Gaunitz, F. (2010). 4-Aminoethylamino-emodin–a novel potent inhibitor of GSK-3beta–acts as an insulin-sensitizer avoiding downstream effects of activated beta-catenin. J. Cell. Mol. Med. *14*, 1276–1293.

Gielisch, I., and Meierhofer, D. (2015). Metabolome and proteome profiling of complex I deficiency induced by rotenone. Journal of proteome research *14*, 224–235.

Gurley, K.A., and Sánchez Alvarado, A. (2008). Stem cells in animal models of regeneration. In StemBook (Harvard Cell Stem Institute).

Hammad, S., Hoehme, S., Friebel, A., Recklinghausenvon, I., Othman, A., Begher-Tibbe, B., Reif, R., Godoy, P., Johann, T., Vartak, A., et al. (2014). Protocols for staining of bile canalicular and sinusoidal networks of human, mouse and pig livers, three-dimensional reconstruction and quantification of tissue microarchitecture by image processing and analysis. Archives of toxicology *88*, 1161–1183.

Hofmann, U., Maier, K., Niebel, A., Vacun, G., Reuss, M., and Mauch, K. (2008). Identification of metabolic fluxes in hepatic cells from transient 13C-labeling experiments: Part I. Experimental observations. Biotechnology and bioengineering *100*, 344–354.

Kalderon, D. (2002). Similarities between the Hedgehog and Wnt signaling pathways. Trends Cell Biol. *12*, 523–531.

Katoh, Y., and Katoh, M. (2006). WNT antagonist, SFRP1, is Hedgehog signaling target. Int. J. Mol. Med. *17*, 171–175.

Kietzmann, T. (2017). Metabolic zonation of the liver: The oxygen gradient revisited. Redox Biol. *11*, 622–630.

Kietzmann, T. (2019). Liver Zonation in Health and Disease: Hypoxia and Hypoxia-Inducible Transcription Factors as Concert Masters. Int. J. Mol. Sci. *20*, E2347.

Klingmüller, U., Bauer, A., Bohl, S., Nickel, P.J., Breitkopf, K., Dooley, S., Zellmer, S., Kern, C., Merfort, I., Sparna, T., et al. (2006). Primary mouse hepatocytes for systems biology approaches: a standardized in vitro system for modelling of signal transduction pathways. Syst. Biol. (Stevenage) *153*, 433–447.

Krämer, A., Green, J., Pollard, J., Jr., and Tugendreich, S. (2014). Causal analysis approaches in Ingenuity Pathway Analysis. Bioinformatics *30*, 523–530.

Kulak, N.A., Pichler, G., Paron, I., Nagaraj, N., and Mann, M. (2014). Minimal, encapsulated proteomic-sample processing applied to copy-number estimation in eukaryotic cells. Nature methods *11*, 319–324.

Li, B., Cao, Y., Meng, G., Qian, L., Xu, T., Yan, C., Luo, O., Wang, S., Wei, J., Ding, Y., and Yu, D. (2019). Targeting glutaminase 1 attenuates stemness properties in hepatocellular carcinoma by increasing reactive oxygen species and suppressing Wnt/beta-catenin pathway. EBioMedicine *39*, 239–254.

Machado, M.V., and Diehl, A.M. (2016). Hedgehog signaling in the liver. In Signaling pathways in liver diseases, J.-F. Dufour and P.-A. Clavien, eds. (John Wiley & Sons), pp. 262–274.

Maier, K., Hofmann, U., Reuss, M., and Mauch, K. (2010). Dynamics and control of the central carbon metabolism in hepatoma cells. BMC systems biology *4*, 54.

Marbach-Breitrück, E., Matz-Soja, M., Abraham, U., Schmidt-Heck, W., Sales, S., Rennert, C., Kern, M., Aleithe, S., Spormann, L., Thiel, C., et al. (2019). Tick-tock hedgehog-mutual crosstalk with liver circadian clock promotes liver steatosis. J. Hepatol. *70*, 1192–1202.

Matz-Soja, M., Aleithe, S., Marbach, E., Böttger, J., Arnold, K., Schmidt-Heck, W., Kratzsch, J., and Gebhardt, R. (2014). Hepatic Hedgehog signaling contributes to the regulation of IGF1 and IGFBP1 serum levels. Cell Commun. Signal. *12*, 11.

Matz-Soja, M., Rennert, C., Schönefeld, K., Aleithe, S., Boettger, J., Schmidt-Heck, W., Weiss, T.S., Hovhannisyan, A., Zellmer, S., Klöting, N., et al. (2016). Hedgehog signaling is a potent regulator of liver lipid metabolism and reveals a GLI-code associated with steatosis. eLife *5*, e13308.

Meng, X., Poon, R., Zhang, X., Cheah, A., Ding, Q., Hui, C.C., and Alman, B. (2001). Suppressor of fused negatively regulates beta-catenin signaling. J. Biol. Chem. *276*, 40113–40119.

Noubissi, F.K., Yedjou, C.G., Spiegelman, V.S., and Tchounwou, P.B. (2018). Cross-Talk between Wnt and Hh Signaling Pathways in the Pathology of Basal Cell Carcinoma. Int. J. Environ. Res. Public Health *15*, E1442.

Planas-Paz, L., Orsini, V., Boulter, L., Calabrese, D., Pikiolek, M., Nigsch, F., Xie, Y., Roma, G., Donovan, A., Marti, P., et al. (2016). The RSPO-LGR4/5-ZNRF3/RNF43 module controls liver zonation and size. Nat. Cell Biol. *18*, 467–479.

Preziosi, M., Okabe, H., Poddar, M., Singh, S., and Monga, S.P. (2018). Endothelial Wnts regulate β-catenin signaling in murine liver zonation and regeneration: A sequel to the Wnt-Wnt situation. Hepatol. Commun *2*, 845–860.

Queiroz, K.C.S., Tio, R.A., Zeebregts, C.J., Bijlsma, M.F., Zijlstra, F., Badlou, B., de Vries, M., Ferreira, C.V., Spek, C.A., Peppelenbosch, M.P., and Rezaee, F. (2010). Human plasma very low density lipoprotein carries Indian hedgehog. J. Proteome Res. *9*, 6052–6059.

Rocha, A.S., Vidal, V., Mertz, M., Kendall, T.J., Charlet, A., Okamoto, H., and Schedl, A. (2015). The Angiocrine Factor Rspondin3 Is a Key Determinant of Liver Zonation. Cell Rep. *13*, 1757–1764.

Salaritabar, A., Berindan-Neagoe, I., Darvish, B., Hadjiakhoondi, F., Manayi, A., Devi, K.P., Barreca, D., Orhan, I.E., Süntar, I., Farooqi, A.A., et al. (2019). Targeting Hedgehog signaling pathway: Paving the road for cancer therapy. Pharmacol. Res. *141*, 466–480.

Schindelin, J., Arganda-Carreras, I., Frise, E., Kaynig, V., Longair, M., Pietzsch, T., Preibisch, S., Rueden, C., Saalfeld, S., Schmid, B., et al. (2012). Fiji: an open-source platform for biological-image analysis. Nature methods *9*, 676–682.

Schmidt-Heck, W., Matz-Soja, M., Aleithe, S., Marbach, E., Guthke, R., and Gebhardt, R. (2015). Fuzzy modeling reveals a dynamic self-sustaining network of the GLI transcription factors controlling important metabolic regulators in adult mouse hepatocytes. Mol. Biosyst. *11*, 2190–2197.

Schönig, K., Schwenk, F., Rajewsky, K., and Bujard, H. (2002). Stringent doxycycline dependent control of CRE recombinase in vivo. Nucleic Acids Res. *30*, e134.

Sekine, S., Lan, B.Y.-A., Bedolli, M., Feng, S., and Hebrok, M. (2006). Liver-specific loss of beta-catenin blocks glutamine synthesis pathway activity and cytochrome p450 expression in mice. Hepatology *43*, 817–825.

Sethi, J.K., and Vidal-Puig, A. (2010). Wnt signalling and the control of cellular metabolism. Biochem. J. *427*, 1–17.

Shibata, H., Toyama, K., Shioya, H., Ito, M., Hirota, M., Hasegawa, S., Matsumoto, H., Takano, H., Akiyama, T., Toyoshima, K., et al. (1997). Rapid colorectal adenoma formation initiated by conditional targeting of the Apc gene. Science *278*, 120–123.

Song, L., Li, Z.-Y., Liu, W.-P., and Zhao, M.-R. (2015). Crosstalk between Wnt/β-catenin and Hedgehog/Gli signaling pathways in colon cancer and implications for therapy. Cancer Biol. Ther. *16*, 1–7.

Starruß, J., Backde, W., Brusch, L., and Deutsch, A. (2014). Morpheus: a user-friendly modeling environment for multiscale and multicellular systems biology. Bioinformatics (Oxford, England) *30*, 1331–1332.

Ueberham, E., Glöckner, P., Göhler, C., Straub, B.K., Teupser, D., Schönig, K., Braeuning, A., Höhn, A.K., Jerchow, B., Birchmeier, W., et al. (2015). Global increase of p16INK4a in APC-deficient mouse liver drives clonal growth of p16INK4a-negative tumors. Mol. Cancer Res. *13*, 239–249.

Uhmann, A., Dittmann, K., Nitzki, F., Dressel, R., Koleva, M., Frommhold, A., Zibat, A., Binder, C., Adham, I., Nitsche, M., et al. (2007). The Hedgehog receptor Patched controls lymphoid lineage commitment. Blood *110*, 1814–1823.

Ulloa, F., and Martí, E. (2010). Wnt won the war: antagonistic role of Wnt over Shh controls dorso-ventral patterning of the vertebrate neural tube. Dev. Dyn. *239*, 69–76.

van den Brink, G.R., Bleuming, S.A., Hardwick, J.C.H., Schepman, B.L., Offerhaus, G.J., Keller, J.J., Nielsen, C., Gaffield, W., van Deventer, S.J.H., Roberts, D.J., and Peppelenbosch, M.P. (2004). Indian Hedgehog is an antagonist of Wnt signaling in colonic epithelial cell differentiation. Nat. Genet. *36*, 277–282.

Verdelho Machado, M., and Diehl, A.M. (2018). The hedgehog pathway in nonalcoholic fatty liver disease. Crit. Rev. Biochem. Mol. Biol. *53*, 264–278.

Werth, M., Gebhardt, R., and Gaunitz, F. (2006). Hepatic expression of glutamine synthetase in rats is controlled by STAT5 and TCF transcription factors. Hepatology *44*, 967–975.

Xia, J., Sinelnikov, I.V., Han, B., and Wishart, D.S. (2015). MetaboAnalyst 3.0–making metabolomics more meaningful. Nucleic acids research *43*, W251–7.

Yang, J., Mowry, L.E., Nejak-Bowen, K.N., Okabe, H., Diegel, C.R., Lang, R.A., Williams, B.O., and Monga, S.P. (2014). β-catenin signaling in murine liver zonation and regeneration: a Wnt-Wnt situation!. Hepatology *60*, 964–976.

Zellmer, S., Sickinger, S., Schmidt-Heck, W., Guthke, R., and Gebhardt, R. (2009). Heterogeneous expression of suppressor of cytokine signalling 2 (SOCS-2) in liver tissue. J. Anat. *215*, 176–183.

STAR★METHODS

KEY RESOURCES TABLE

REAGENT or RESOURCE	SOURCE	IDENTIFIER
Antibodies		
Rabbit polyclonal anti-Axin2 (used for: IF)	Abcam	Cat # ab32197, RRID:AB_2290204
Mouse monoclonal anti-ACTB (used for: WB)	Abcam	Cat # ab8224, RRID:AB_449644
Mouse monoclonal anti-CTNNB1 (used for: IHC)	BD Biosciences	Cat # 610154, RRID:AB_397555
Rabbit polyclonal anti-FZD2 (used for: IHC)	Alomone	Cat # AFR-022, RRID:AB_2756591
Rabbit polyclonal anti FZD4 (used for: IHC)	LSBio	Cat # LS-B5723, RRID:AB_10912529
Rabbit polyclonal anti-GLI1 (used for: IHC)	GeneTex	Cat # GTX124274, RRID:AB_11174802
Rabbit polyclonal anti-GLI2 (used for: IHC)	Biozol	Cat # ORB378810
Rabbit polyclonal anti-GLI3 (used for: IHC)	GeneTex	Cat # GTX2605, RRID:AB_425213
Rabbit polyclonal anti-GLUL (used for: IF)	Abcam	Cat # ab49873, RRID:AB_880241
Rabbit polyclonal anti-IHH (used for: IF, IHC)	Abcam	Cat # ab39634, RRID:AB_881366
Rabbit polyclonal anti-PTCH1 (used for: IHC)	LifeSpan	Cat # LS-C122292, RRID:AB_10800195
Rabbit polyclonal anti-PTCH2 (used for: IHC, WB)	LifeSpan	Cat # LS-B301, RRID:AB_2269074
Rabbit polyclonal anti-WNT5a (used for: IHC)	St. John's Laboratory	Cat # StJ26117
Goat biotinylated polyclonal anti-rabbit IgG (used for: IF)	Millipore	Cat # AP132B, RRID:AB_11212148
Extravidine-Cy3 (used for: IF)	Sigma-Aldrich	Cat # E4142
IRDye® 800CW Goat anti-Rabbit (used for: WB)	LI-COR Biosciences	Cat # 926-32211, RRID:AB_621843
IRDye® 680RD Goat anti-Mouse	LI-COR Biosciences	Cat # 926-68070, RRID:AB_10956588
Biological samples		
human liver sections	Christian-Albrechts University/ Leipzig University	N/A
murine liver sections	Leipzig University	N/A
murine hepatocytes	Leipzig University	N/A
Chemical, Peptides and Recombinant Proteins		
Collagenase Type I, CLS I	Biochrom	Cat # C 1-22
Digitonin	Sigma	Cat # D141
INTERFERin®	VWR	Cat # 409-50
rec. IHH	R&D	Cat # 1705-HH-025
rec. SHH	R&D	Cat # 464-SH-025
Critical Commercial Assays		
EnVision+Dual Link System-HRP	Agilent	Cat # K406311-2
iST in-stage tip kit	PreOmics	Cat # P.O.00027
LightCycler® FastStart DNA Master PLUS SYBR Green I	Roche	Cat # 03515869001
Maxima First Strand cDNA Synthesis Kit	Thermo-Fisher	Cat # K1671
peqGOLD RNAPure	VWR	Cat # 732-3312
Proto Script M-MuLV First Strand cDNA Synthesis Kit	New England Biolabs	Cat # E6300L
REVERT Total Protein Stain Kit	LI-COR Biosciences	Cat# P/N 926-11016
Rotor-Gene SYBR® Green PCR Kit	QIAGEN	Cat # 204074
Tyramide SuperBoost Kit	Thermo-Fisher,	Cat # B40915
Tyramide SuperBoost Kit	Thermo-Fisher	Cat # B40922
Deposited Data		
Metabolome analysis data of *Apc*^{WT} versus *Apc*^{homo}, SAC-WT versus SAC-KO and pp versus pc C57Bl6N hepatocyte supernatant	This Paper, LiSyM SEEK	https://seek.lisym.org/data_files/439?code=mpMmEN0lH10LB%2B%2FMkYBAYDKtZKV9dJ%2Fu7wAQ7SIU

(*Continued on next page*)

Continued

REAGENT or RESOURCE	SOURCE	IDENTIFIER
Experimental Models: Organisms/ Strains		
Mouse: Apc^{homo}	Shibata et al., 1997	N/A
Mouse: C57Bl6/N	Medizinisches Experimentelles Zentrum Leipzig	Internal breeding and hosting.
Mouse: SAC-KO	Matz-Soja et al., 2014	N/A
Mouse: IHH-KO	This Paper	N/A
Oligonucleotides for qPCR (murine)		
Actb Forward Primer CATCCGTAAAGACCTCTATGCCAAC	This Paper	N/A
Actb Reverse Primer ATGGAGCCACCGATCCACA	This Paper	N/A
Apc Forward Primer CTCACTTACCGGAGCCAGAC	This Paper	N/A
Apc Reverse Primer GATTCCACAAAGTTCCACATGC	This Paper	N/A
Axin2 Forward Primer TGAAACTGGAGCTGGAAAGC	This Paper	N/A
Axin2 Reverse Primer AGAGGTGGTCGTCCAAAATG	This Paper	N/A
Ccnd1 Forward Primer GAGACCATTCCCTTGACTGC	This Paper	N/A
Ccnd1 Reverse Primer TGGTCTGCTTGTTCTCATCC	This Paper	N/A
Ctnnb1 Forward Primer GCAGCAGCAGTCTTACTTGG	This Paper	N/A
Ctnnb1 Reverse Primer CCCTCATCTAGCGTCTCAGG	This Paper	N/A
See table S5 for additional qPCR primer	This Paper	See Table S5
Apc siRNA GGACUGGUAUUAUGCUCAATT UUGAGCAUAAUACCAGUCCTT	QIAGEN	Cat # Mm_APC_1 (NM_007462)
Ctnnb1 siRNA GGGACGUUCACAACCGGAUUGUAAUA UUACAAUCCGGUUGUGAACGUCCC	Invitrogen	Cat # MSS202664
Gli1 siRNA CCCAACAUGGCAGUGGGUAACAUGAUCA UGUUACCCACUGCCAUGUUGGG	Invitrogen	Cat # MSS712 Gli1
Gli2 siRNA CCACAACCACAACGUUGCUCAGACA UGU CUGAGCAAGCUUGUGGUUGUGG	Invitrogen	Cat # MSS204726 Gli2
Gli3 siRNA UAGCAAGGCCAUCUUGGUCUUCAGG	Invitrogen	Cat # MSS204728 Gli3
See table S6 for additional siRNA sequences	Invitrogen	See Table S6
Recombinant DNA		
GLI1	Promega/ KDRI	FHC07737
GLI2	Promega/ KDRI	FHC07749
GLI3	Promega/ KDRI	FHC07751
Software and Algorithms		
CorelDRAW	Corel	https://www.coreldraw.com/en/
Fiji (ImageJ)	Schindelin et al., 2012	https://imagej.net/Fiji
R/iGraph		https://igraph.org
Image Studio Light	Li-Cor	https://www.licor.com/bio/image-studio-lite/
Ingenuity Pathway Analysis	QIAGEN	https://www.qiagenbioinformatics.com/products/ingenuity-pathway-analysis/
MaxQuant	Cox and Mann, 2008	https://www.maxquant.org/
MetaboAnalyst	Xia et al., 2015	https://www.metaboanalyst.ca/
PRISM7	GraphPad Software	https://www.graphpad.com/
Rotorgene Q Software	QIAGEN	http://www.qiagen.com/us/shop/automated-solutions/pcr-instruments/rotor-gene-q/
R		http://www.R-project.org/
TiQuant	Friebel et al., 2015	https://www.hoehme.com/software/9-software/8-tiquant

LEAD CONTACT AND MATERIALS AVAILABILITY

Further information and requests for resources and reagents should be directed to and will be fulfilled by the Lead Contact, Madlen Matz-Soja (madlen.matz@medizin.uni-leipzig.de). All mouse lines generated in this study are available from the Lead Contact with a completed Materials Transfer Agreement.

EXPERIMENTAL MODEL AND SUBJECT DETAILS

Human subjects

For human histology liver material from male and female patients with a NAFLD activity score (NAS) from 0-1 were included. Specimen collection for all samples were approved by either Christian-Albrechts University (AZ: D 425/07; A 110/99) or Leipzig University (AZ: 177/16-Ik) ethics committee. The informed consent was obtained from all subjects. The human liver material in this study was obtained from male patients.

Murine subjects

For the study of Wnt/Hh signaling in the physiological state, 3 month old male C57BL6/N mice were used. For the investigation of the inactivated Hh pathway and activated Wnt signaling in this study two transgenic mouse models were used. The SAC mice with a hepatocyte-specific deletion of *Smo with* the expression of the Cre recombinase is under the control of the mouse albumin promoter and the α-fetoprotein enhancer (Matz-Soja et al., 2014) and the Apc^{homo} mice bearing a homozygous floxed exon 14 in the *Apc* allele (Shibata et al., 1997). SAC-WT, SAC-KO as well as APC-WT and APC-KO mice where sacrificed at the age of 12 weeks.

Triple transgenic mice allowing conditional hepatocyte-specific ablation of Ihh in response to exposure to doxycycline were generated by crossing the 129S4-Ihhtm1Blan/J mice (Jackson Laboratories) possess loxP sites flanking exon 1 of the targeted gene (Uhmann et al., 2007) with double transgenic LC-1/rTALAP −1 mice (Schönig et al., 2002). For inducing ablation of Ihh, mice were grown up for 8 weeks under normal conditions. Then, expression of Cre recombinase was induced by adding doxycycline hydrochloride (2 mg/ml) to the drinking water for a period of 10 days. Mice where sacrificed at the age of 12 weeks.

The mice were maintained in a pathogen-free facility on a 12:12 h light–dark cycle, according to the German guidelines and the world medical association declaration of Helsinki for the care and safe use of experimental animals (permission numbers: C57BL6/N mice: N03/14; SAC mice: T04/14, TVV 11; APC mice: T37/12 ; IHH mice: TVV44/16).

METHOD DETAILS

Maintenance of the mice and feeding

The mice were maintained in a pathogen-free facility on a 12:12 h LD cycle. The animals had free access to regular chow (ssniff® M-Z V1124-0 composed of 22.0% protein, 50.1% carbohydrate, 4.5% fat; usable energy: 13.7 kJ/g; ssniff® Spezialdiäten GmbH, Germany) and tap water throughout life. The mice were studied at 3 months of age and sacrificed between 9 and 11 am after administration of an anesthetic mixture of ketamine, xylazine and atropine.

Isolation and cultivation of primary mouse hepatocytes

The primary hepatocytes were isolated from mice by a collagenase perfusion technique as described before (Klingmüller et al., 2006; Gebhardt et al., 2010). By differential centrifugation the cell suspension was cleared of non-parenchymal cells (Matz-Soja et al., 2014). Immediately after isolation the cells are incubated for 3-4 hours in Williams E medium (Millipore, F1115) for adherence with: 2 mM L-Glutamine, 42 μM Penicilin, 42 μM Streptomycin, 100 nM Dexamethasone as well as 10% (v/v) fetal calf serum. Afterward there is a medium change with the same Williams E medium without fetal calf serum. In this medium the cells are incubated. Medium is changed every 24 hours. The serum-free medium was used for the analyses of the extracellular metabolites after the first 24 h of incubation.

Isolation of primary periportal and pericentral mouse hepatocytes

Periportal and pc hepatocytes were isolated using digitonin-collagenase perfusion technique as described before (Burger et al., 1989; Gebhardt 1998). In brief, for harvesting the respective cell fraction the liver was injected by digitonin for destruction of hepatocytes from the opposite porto-central area. Digitonin injection was performed either retrograde (over vena cava inferior) for isolation of pp hepatocytes or anterograde (over vena portae) for isolation of pc hepatocytes. Following the liver was perfused with collagenase. The cell suspension was cleared of non-parenchymal cells via differential centrifugation (Matz-Soja et al., 2014). Hepatocyte culture conditions beyond seeding were performed analog to mixed cell population (see above).

RNA isolation and quantitative real-time PCR (qPCR)

Total RNA from hepatocytes and liver tissue were extracted by peqGOLD RNAPure (VWR). The RNA was reverse transcribed with the IM Prom II reverse transcriptase (Promega, Germany) and the Proto Script M-MuLV First Strand cDNA Synthesis Kit (New England Biolabs) according to the manufacturer's instructions. The resulting cDNA was quantified in duplicates by qPCR using the Rotor-

Gene SYBR® Green PCR Kit and a Rotor-Gene Q (QIAGEN, Germany), as well as the LightCycler® 2.0 Instrument and the LightCycler® FastStart DNA Master PLUS SYBR Green I (Roche, Germany) according to the manufacturer's instructions. For each target a gene-specific and intron-spanning primer was designed with Primer 3. For genes with no possibility for intron-spanning primer Maxima First Strand cDNA Synthesis Kit (Thermo-Fisher, USA) was used. Using the standard curve method, the absolute amount of the specific PCR products for each primer set was quantified. *Actb* (β-Actin) was amplified from each sample for normalization as reference gene.

RNA interference

For all siRNA mediated knockdown experiments isolated hepatocytes from non-transgenic male C57BL/6N mice were used. The specific siRNA and the respective nonsense oligo control siRNA were purchased from Invitrogen, Germany. The hepatocytes were seeded at a density of 100,000 cells per well on 12-well plates. After 4 h, the cells were transfected with the respective siRNA (10 nM) with INTERFERin® (VWR, Germany) according to the manufacturer's instructions. 24 h after transfection, the medium was changed, and fresh medium without the siRNA was added. The changes in gene expression were analyzed by qPCR 48 h post transfection.

GLI overexpression experiments

After isolation, hepatocytes from male C57BL/6N mice at the age of 12 weeks were cultivated at 0.25 Mio. cells per well in 6-well plates in 1.5 ml medium (William's Medium E enriched with 10% fetal calf serum, 2 mM L-glutamine, 100 nM dexamethasone and Pen/Strep). After 3-4 h medium was changed and the transfection was performed analog (Matz-Soja et al., 2016).

In vitro IHH and SHH gain off function analysis

After isolation, hepatocytes from male C57BL/6N mice at the age of 12 weeks were seeded at a density of 100,000 cells per well on 12-well plates in 1.0 ml medium (William's Medium E enriched with 10% fetal calf serum, 2 mM L-glutamine, 100 nM dexamethasone and Pen/Strep). After 3-4 h medium was changed and fresh media without fetal calf serum, but added recombinant protein for murine IHH (rec. IHH, R&D, 1705-HH-025) and SHH (rec. SHH, R&D, 464-SH-025) and PBS as control was used. 24 h after treatment, the medium was changed, and fresh medium with the recombinant proteins was added. The changes in gene expression were analyzed by qPCR 48 h post treatment.

Immunohistochemistry

Immunohistochemistry on paraffin sections (3 μm) was performed as previously described (Zellmer et al., 2009). In brief, the sections were deparaffinized, rehydrated and subsequently boiled in citric buffer (0.01 M sodium citrate, pH 6.0) or Tris/EDTA buffer (10 mM Tris; 1 mM EDTA). Next the slides were incubated for 1 h min in 5% goat serum (Sigma-Aldrich, Germany) to block nonspecific binding. The following primary antibodies were used: anti AXIN2 (1:1000; Abcam, ab32197, UK), anti CTNNB1 (1:500; Transduction Laboratories, 610054, USA), anti FZD2 (1:700; Alomone, AFR-022, Israel), anti FZD4 (1:500; LSBio, LS-B5723, USA) anti GLI1 (1:1500; GeneTex, GTX124274, USA), anti GLI2 (1:140; Biozol, ORB378810, Germany) anti GLI3 (1:1000; GeneTex, GTX26050, USA), Sigma, Germany), anti GS (1:1000; Abcam, ab49873, UK), anti IHH (1:600; Abcam, ab39634, UK), anti PTCH1 (1:1000; LSBio, LS-C122292, USA), anti PTCH2 (1:1000; LSBio, LS-B301, USA), anti WNT5a (1:500; St. John's Laboratory, StJ26117, UK). Peroxidase staining was performed using the EnVision+Dual Link System-HRP (Agilent, K406311-2, USA) according to manufacturer instructions. For immune fluorescence stainings Tyramide Super Boost Kits were used according to the manufacturer instructions (Thermo-Fisher, B40922/ B40915, USA) and following antibodies were used: biotinylated goat anti-rabbit IgG (Millipore, AP132B, Germany), Extravidine Cy3 (1:800; Sigma, E4142, Germany), goat anti mouse Cy3 (1:1000; Dianova, 115-167-003, Germany).

TiQuant - Protein quantification

Immunofluorescence double staining of AXIN2/GLUL on Apc^{WT} versus Apc^{homo} and on SAC-WT versus SAC-KO mice liver sections, were analyzed by the modular image analysis software *TiQuant* (Friebel et al., 2015). *TiQuant* provides traditional pixel based image processing pipelines suited for specific applications (Hammad et al., 2014) as well as a general supervoxel-based machine learning approach to segment two- and three-dimensional images. The latter method was used for segmentation of the micrographs at hand. First, an image is split into visually distinct, similarly sized regions, the so called supervoxels, using the SLIC0 algorithm (Achanta et al., 2012). Each supervoxel is characterized by a set of features, comprising local, and neighborhood color histograms as well as texture and gradient descriptors. An image is then annotated partially to provide training data in the form of labeled supervoxels. A Random Forest classifier is fitted to the training data and subsequently used to predict class membership probabilities for each supervoxel given their respective feature set. Segmentations are then inferred from these probabilities, and post-processed using the watershed algorithm to separate clustered objects. Based on the obtained segmentations, the area of each staining in each individual micrograph was measured by pixel counting, and then statistically merged and analyzed.

Western Blot

The isolated hepatocytes were lysed in RIPA buffer using the Precellys 24 homogenizer. Equal quantities of protein lysate were separated by an 8% SDS-PAGE followed by wet immunoblotting transfer on nitrocellulose membrane (Roth, Germany). The membrane

was blocked in Odyssey® Blocking Buffer (LI-COR Biosciences) and incubated with primary antibodies against PTCH2 (1:500; LSBio, LS-B301, USA) and ACTB (1:1000; Abcam, ab8224, UK). Secondary antibodies IRDye® 800CW Goat anti-Rabbit (LI-COR Biosciences, 926-32211, USA) and IRDye® 680RD Goat anti-Mouse (1:10000; LI-COR Biosciences, 926-68070, USA) were used for visualization with the Odyssey Fc imager (LI-COR Biosciences). For normalization the amount of total protein was measured via REVERT Total Protein Stain (LI-COR Biosciences) and analyzed by Image Studio 5.2 Software (LI-COR Biosciences).

Affymetrix chip array

Microarray analysis was conducted using liver material from IHH-WT and IHH-KO mice (n = 4 per genotype), at the microarray core facility of the Interdisziplinäres Zentrum für klinische Forschung (IZKF) Leipzig (Faculty of Medicine, Leipzig University) described by Zellmer et al. (2009). Briefly, GeneChip Mouse Genome 430 2.0 Arrays (Affymetrix) were used for hybridization. The gene expression data were pre-processed by Probe-level Linear Models using the 'affyPLM' packages of the Bioconductor Software.

Metabolome

Proteinogenic AA, ornithine, urea, pyruvate, acetoacetate, hydroxybutyrate, fumarate, α-ketoglutarate, malate, and citrate were determined by GC–MS analysis as described (Hofmann et al., 2008; Maier et al., 2010). Lactate and bile acids were determined by negative electrospray (ESI) LC–MS/MS in multiple-reaction-monitoring (MRM) mode on an Agilent 6460 triple quadrupole mass spectrometer (Agilent, Waldbronn, Germany) coupled to an Agilent 1200 HPLC system. Ion pairing RP-HPLC separation of lactate was performed similar to a described method (Maier et al., 2010), and MRM transitions were 92 → 45 and 89 → 43 for lactate and the internal standard [13C3]lactate, respectively. The bile acids β-muricholate, tauromuricholate, and taurocholate were separated on a Poroshell 120 EC-C18 column (100 × 2.1 mm, 2.7 μm particle size, Agilent) using a gradient of (A) 12 mm ammonium acetate in water, and (B) acetonitrile as mobile phases at a flow rate of 0.5 ml/min. MRM transitions were 407.3 → 407.3 for β-muricholate, 514.3 → 80 for taurocholate and tauromuricholate, and 518.3 → 80 for the internal standards [2H4]tauromuricholate and [2H4] taurocholate. The statistical and enrichment analysis of the obtained data was performed via the MetaboAnalystR software. In this regards the samples were normalized by a pooled sample from the WT group in case of the transgenic animals and the pp group in case of the hepatocytes from the pc and pp zone. After normalization the data were log transformed. For the quantitative enrichment analysis the metabolic pathway associated metabolic library was chosen. The global test was used to analyze the Q-statistics for each metabolite set.

Sample preparation for proteome profiling

The flow cytometry sorted cells were lysed at 95°C for 10 min in lysis buffer containing 1% sodium deoxycholate (SDC), 10 mM tris(2-carboxyethyl)phosphine (TCEP), 40 mM chloroacetamide (CAA), and 100 mM Tris pH 8.5. Incubation was followed by 5 min sonication. The lysates were digested and purified using the preOmics in-stage tip kit (iST kit 96x, Martinsried, Germany). Samples were eluted sequentially in three fractions using the SDB-RPS-1 and −2 buffers (Kulak et al., 2014) and the elution buffer provided by preOmics for subsequent analysis on a nanoLC-MS.

LC-MS instrument settings for shotgun proteome profiling and data analysis

LC−MS/MS was carried out by nanoflow reverse phase liquid chromatography (Dionex Ultimate 3000, Thermo Scientific, Waltham, MA) coupled online to a Q-Exactive HF Orbitrap mass spectrometer (Thermo Scientific, Waltham, MA). The LC separation was performed using a PicoFrit analytical column (75 μm ID × 55 cm long, 15 μm Tip ID (New Objectives, Woburn, MA) in-house packed with 3-μm C18 resin (Reprosil-AQ Pur, Dr. Maisch, Ammerbuch-Entringen, Germany), as reported previously (Gielisch and Meierhofer, 2015). Briefly, peptides were eluted using a gradient from 3.8 to 50% solvent B in solvent A over 121 min at 266 nL per minute flow rate. Solvent A was 0.1% formic acid and solvent B was 79.9% acetonitrile, 20% water, 0.1% formic acid. Nanoelectrospray was generated by applying 3.5 kV. A cycle of one full Fourier transformation scan mass spectrum (300−1750 m/z, resolution of 60,000 at m/z 200, AGC target 1e6) was followed by 12 data-dependent MS/MS scans (resolution of 30,000, AGC target 5e5) with a normalized collision energy of 25 eV. In order to avoid repeated sequencing of the same peptides a dynamic exclusion window of 30 s was used. In addition, only the peptide charge states between two to eight were sequenced.

Raw MS data were processed with MaxQuant software (1.5.7.4) (Cox and Mann, 2008) with the Andromeda search engine (Cox and Mann, 2008) and the mouse UniProtKB with 51,416 entries released in 03/2016. A false discovery rate (FDR) of 0.01 for proteins and peptides, a minimum peptide length of 7 AA, a mass tolerance of 4.5 ppm for precursor and 20 ppm for fragment ions were required. A maximum of two missed cleavages was allowed for the tryptic digest. Cysteine carbamidomethylation was set as fixed modification, while N-terminal acetylation and methionine oxidation were set as variable modifications. Determined up- or downregulated proteins in the transgenic SAC-KO and Apc^{homo} mice were overlaid onto a global molecular network developed from information contained in the Ingenuity Pathways Knowledge Base. Networks of these focus genes were then algorithmically generated based on their interrelationships.

In vitro knockdown experiments data analysis

Gene expression responses of ten Hh and 15 Wnt pathway genes were considered for selected siRNA knockdowns of 9 Hh (*Ptch1, Ptch2, Ptch1/2, Smo, Fused, Sufu, Gli1, Gli2, Gli3*) and 2 Wnt pathway genes (*Ctnnb1, Apc*). A heatmap was created that provides a

global overview of expression responses associated with the specific knockdowns (Figure S3A). Columns represent responses of individual genes to a specific knockdown. Rows represent the expression response of a specific gene across the different knockdowns. Inhibition (blue), no change (gray) and activation (red) of a gene in response to a knockdown are highlighted and pathway memberships of the individual genes are shown (green: Hedgehog, orange: Wnt).

Similarities between the different responses were analyzed by computing correlations between the response-specific gene expression profiles (R function cor with option use = "pairwise.complete.obs" to account for missing values). This was done for each pair of genes and the resulting correlation matrix was visualized as heatmap to identify subclusters.

The log2-fold expression changes enable to determine genes that tend to respond to knockdown of a specific gene. For each knockdown, one can determine genes whose absolute log2-fold expression change is greater than a fixed threshold. We used a stringent log2-fold expression cutoff of 1 and a less stringent cutoff of 0.5 to determine which knocked down genes putatively influence the expression of other genes (Figure S3B). Corresponding interaction networks were visualized using the R package igraph.

Details of the mathematical model

We use the following dependent variables in the model:

- a scalar field $w(\vec{x},t)$representing Wnt ligand concentration
- a scalar field $b(\vec{x},t)$representing intracellular Wnt pathway protein (AXIN) concentration
- a scalar field $h(\vec{x},t)$representing sonic hedgehog ligand concentration
- a scalar field $i(\vec{x},t)$representing indian hedgehog ligand concentration
- a scalar field $g(\vec{x},t)$ representing GLI3 protein concentration

We also use the quantities *a* for APC and *c* for SMO, but they are assumed to be spatially and temporally constant and only act as adjustable parameters in the equations. As we do not attempt a quantitative analysis at this point, parameter values were chosen manually to demonstrate sufficiency of the considered interactions for reproducing spatial staining patterns.

All variables are considered as dimensionless quantities, they are not scaled to any particular unit and their absolute magnitudes need not be compared to each other.

A set of partial differential equations that is informed by measurements and qualitative observations is used for determining spatial patterns of these quantities. The equations are then solved numerically for steady-state solutions using Morpheus (Starruß et al., 2014).

For demonstration purposes we use a quadratic two-dimensional domain although for many conclusions a one-dimensional domain is already sufficient. A grid size of 250x250 pixels is used (with one pixel representing 0.1 length units), a hexagonal central vein pattern is superimposed on this grid. Each central vein has a radius of 5 pixels, the distance between two central veins is 100 pixels.

We start with the equation for *w*:

$$w_t = I\left(\vec{x}\right) - k_1 w + D_w \nabla^2 w$$

Here $I(\vec{x})$ denotes the spatial-dependent production term of w. $I(\vec{x})$ is set 1 at a central vein and 0.001 elsewhere. Hence, the equation assumes production of *w* predominantly at the central vein, diffusion and degradation.

The next equation for *b* reads as:

$$b_t = b(w-a)\left(\frac{1}{1+k_2 h} - b\right) + D_b \nabla^2 b$$

We assume activation of *b* by *w*, inactivation by *a*, expression limitation by *h* and degradation. The activation by *w* (Wnt) and inactivation by *a* (APC) is very plausible as APC is known to block Wnt signaling in other systems (Gurley and Sánchez Alvarado, 2008). The expression limitation by *h* is motivated by the SAC-KO experiments that resulted in an increase of many Wnt pathway genes (see Figure 6A).

The next equation is for sonic hedgehog *h*:

$$h_t = k_3 c - k_4 w h + D_h \nabla^2 h$$

We assume SMO dependent expression (increasing SMO increases SHH), this is justified from the *in-vitro* data. Further we assume Wnt dependent degradation (increasing WNT decreases SHH) and diffusion. The latter assumption is crucial for the increased periportal *h*. Although it is not directly proven by an experiment it is indirectly supported by the negative correlation of WNT and SHH (see Figure 7).

The equation for *i* reads as:

$$i_t = b c^2 - k_5 i$$

This assumes production of *i* that depends on *b* and strongly on *c* (a linear term with respect to *c* does not work as well) and degradation. These choices are informed by the *in-vitro Apc* and *Smo* knockout.

And finally, the equation for g is:

$$g_t = k_6 i + k_7 h - k_8 g + D_g \nabla^2 g$$

Here we assume expression induced by i and h (the hedgehog ligands), degradation and diffusion. The assumption is supported by the fact that GLI3 is logically downstream of the two hedgehog ligands. The assumption is also supported by similar behavior of *Gli3, Shh* and *Ihh* in the *in-vitro* knockdown experiments.

The equations are integrated until a steady-state is achieved. The only spatial information that the model receives is the location of the central veins via the function $I(\vec{x})$. This information produces a pericentral-periportal gradient in w and subsequently creates the spatial patterns in all the other quantities.

For the control $a = 0.2$ and $c = 1.0$ are sedused. For Apc^{homo} we use $a = 0.1$ and for SAC-KO we use $c = 0.3$.

In the simulations for the human samples we used the following settings: all equations are structurally the same but we use different parameter values in the equation for w. I(x) is defined to be 1.4 at the central vein and 0.4 elsewhere, k_1 = 1.0 and D_w = 0.2. The parameters for the mathematical model were fitted manually (Table S7).

QUANTIFICATION AND STATISTICAL ANALYSIS

Most experiments were repeated 2-3 times with different quantities of biological replicates (n = 3 to 11) as indicated in each figure. The number of technical replicates depended on the type of experiment and was mostly duplicates or triplicates. Outliers were identified with the ROUT test of GraphPad Prism 7 (aggressiveness 0.5%). Values are plotted as average of biological replicates ± standard error of the mean. The statistical evaluation was performed with the unpaired Student's t test. The null hypothesis was rejected at the $p < 0.05$ (*); $p < 0.01$ (**), $p < 0.001$ (***) and $p < 0.0001$ (****) levels.

DATA AND CODE AVAILABILITY

The proteome dataset supporting the current study have not been deposited in a public repository because the dataset is not public because further publications based on this data are in progress, but are available from the corresponding author on request. In case of the metabolom raw data please use the following link: https://seek.lisym.org/data_files/439?code=mpMmEN0lH10LB%2B%2FMkYBAYDKtZKV9dJ%2Fu7wAQ7SIU. The published article includes all other datasets generated or analyzed during this study.